

IMAGING VIBRIO CHOLERAE INVASION AND DEVELOPING NEW TOOLS FOR  
3D MICROSCOPY OF LIVE ANIMALS

by

SAVANNAH LEE LOGAN

A DISSERTATION

Presented to the Department of Physics  
and the Graduate School of the University of Oregon  
in partial fulfillment of the requirements  
for the degree of  
Doctor of Philosophy

December 2018

DISSERTATION APPROVAL PAGE

Student: Savannah Lee Logan

Title: Imaging *Vibrio Cholerae* Invasion and Developing New Tools for 3D Microscopy of Live Animals

This dissertation has been accepted and approved in partial fulfillment of the requirements for the Doctor of Philosophy degree in the Department of Physics by:

Benjamín Alemán	Chairperson
Raghuveer Parthasarathy	Advisor
Tristan Ursell	Core Member
Karen Guillemin	Institutional Representative

and

Janet Woodruff-Borden	Vice Provost and Dean of the Graduate School
-----------------------	--

Original approval signatures are on file with the University of Oregon Graduate School.

Degree awarded December 2018

© 2018 Savannah Lee Logan

## DISSERTATION ABSTRACT

Savannah Lee Logan

Doctor of Philosophy

Department of Physics

December 2018

Title: Imaging *Vibrio Cholerae* Invasion and Developing New Tools for 3D Microscopy of Live Animals

All animals harbor microorganisms that interact with each other and with their hosts. These microorganisms play important roles in health, disease, and defense against pathogens. The microbial communities in the intestine are particularly important in preventing colonization by pathogens; however, this defense mechanism and the means by which pathogens overcome it remain largely unknown. Moreover, while the composition of animal-associated microbial communities has been studied in great depth, the spatial and temporal dynamics of these communities has only recently begun to be explored.

Here, we use a transparent model organism, larval zebrafish, to study how a human pathogen, *Vibrio cholerae*, invades intestinal communities. We pay particular attention to a bacterial competition mechanism, the type VI secretion system (T6SS), in this process. *In vivo* 3D fluorescence imaging and differential contrast imaging of transparent host tissue allow us to establish that *V. cholerae* can use the T6SS to modulate the intestinal mechanics of its host to displace established bacterial communities, and we demonstrate that one part of the T6SS apparatus, the actin crosslinking domain, is responsible for this function.



Next, we develop an automated high-throughput light sheet fluorescence microscope to allow rapid imaging of bacterial communities and host cells in live larval zebrafish. Light sheet fluorescence microscopy (LSFM) has been limited in the past by low throughput and tedious sample preparation, and our new microscope features an integrated fluidic circuit and automated positioning and imaging to address these issues and allow faster collection of larger datasets, which will considerably expand the use of LSFM in the life sciences. This microscope could also be used for future experiments related to bacterial communities and the immune system.

The overarching theme of the work in this dissertation is the use and development of advanced imaging techniques to make new biological discoveries, and the conclusions of this work point the way toward understanding pathogenic invasion, maximizing the use of LSFM in the life sciences, and gaining a better grasp of host-associated bacterial community dynamics.

This dissertation includes previously published and unpublished co-authored material.

## CURRICULUM VITAE

NAME OF AUTHOR: Savannah Lee Logan

### GRADUATE AND UNDERGRADUATE SCHOOLS ATTENDED:

University of Oregon, Eugene, OR  
University of Oklahoma, Norman, OK

### DEGREES AWARDED:

Doctor of Philosophy, Physics, 2018, University of Oregon  
Bachelor of Science, Astrophysics, 2013, University of Oklahoma  
Bachelor of Musical Arts, 2013, University of Oklahoma

### AREAS OF SPECIAL INTEREST:

Host-microbe interactions  
Light sheet fluorescence microscopy  
Instrument design  
Pathogenic invasion  
The immune system

### PROFESSIONAL EXPERIENCE:

Graduate Research Assistant, Parthasarathy Lab, University of Oregon, Eugene,  
Oregon, 2014-2018  
  
Graduate Teaching Fellow, Department of Physics, University of Oregon,  
Eugene, Oregon, 2013-2015

### GRANTS, AWARDS, AND HONORS:

Teaching Engagement Program Core Certificate, University of Oregon, 2018  
  
Fowler Prize, University of Oklahoma, 2013  
  
J. Clarence Karcher Scholarship, University of Oklahoma, 2012  
  
National Merit Scholarship, 2008

PUBLICATIONS:

Logan, S.L., Dudley, C., Baker, R.P., Taormina, M.J., Hay, E.A., and Parthasarathy, R. (2018). *PLoS ONE*. (in press).

Logan, S.L., Thomas, J., Yan, J., Baker, R.P., Shields, D.S., Hammer, B.K., Xavier, J.B., and Parthasarathy, R. (2018). *Proceedings of the National Academy of Sciences*, 201720133; DOI:10.1073/pnas.1720133115.

Wiles, T.J., Jemielita, M., Baker, R.P., Schlomann, B.H., Logan, S.L., Ganz, J., Melancon, E., Eisen, J.S., Guillemin, K., and Parthasarathy, R. (2016). *PLoS Biology*, 14(7), 1-24. <https://doi.org/10.1371/journal.pbio.1002517>.

## ACKNOWLEDGMENTS

The work in this dissertation, as well as my success in graduate school, would not have been possible without the support of my advisor, Dr. Raghuv eer Parthasarathy. His mentorship and guidance have been essential for my development as a scientist and as a person. I would also like to thank the many members of the Parthasarathy Lab who have helped with this research and who have made working in the lab more fun, including Christopher Dudley, Mike Taormina, Matt Jemielita, Tristan Hormel, Ryan Baker, Brandon Schlomann, Teddy Hay, Philip Jahl, and Deepika Sundarraman.

Thank you to my thesis committee for supporting my research and for offering your insights regarding research directions and career paths. I would also like to thank Jason Schreiner and Elly Vandegrift for helping me explore my interests in teaching, and Dan Crowe for the many fun times in the Outdoor Program. Thanks also to Brian Hammer and Joao Xavier for helping me see my work from other perspectives and for contributing to the research in this dissertation.

I would also like to thank the many friends and climbing partners who have supported me throughout graduate school, especially Ben Strickland, Amelia Rhodewalt, Jordan Palamos, Haley Sharp, Andrew Blaikie, Kentaro Hoegar, Ariel Steele, and the other members of my incoming class. Thanks you also to Dan Stringer and Bacon (the dog) for many fun adventures.

Finally, I would like to thank my family for always supporting me and encouraging me to pursue my interests. I wouldn't have gotten this far without you.

## TABLE OF CONTENTS

Chapter	Page
I. MICROBES, HOSTS, PATHOGENS, AND THE IMMUNE SYSTEM .....	1
1.1 Introduction.....	1
1.2 Model organisms.....	2
1.3 Pathogens, colonization resistance, and microbial competition mechanisms.....	5
1.4 The immune system, neutrophils, and inflammation.....	6
1.5 Discussion.....	7
II. LIGHT SHEET FLUORESCENCE MICROSCOPY .....	9
2.1 Introduction.....	9
2.2 Current work in light sheet fluorescence microscopy.....	11
2.3 Limitations of current light sheet fluorescence microscopes.....	15
2.4 Discussion.....	16
III. THE VIBRIO CHOLERAE TYPE VI SECRETION SYSTEM CAN MODULATE HOST INTESTINAL MECHANICS TO DISPLACE GUT BACTERIAL SYMBIONTS .....	17
3.1 Introduction: <i>Vibrio cholerae</i> and the type VI secretion system .....	17
3.2 Human-derived <i>Vibrio cholerae</i> colonizes the larval zebrafish intestine but exhibits weak intra-species T6SS-mediated killing <i>in vivo</i> .....	22
3.3 Constitutive expression of the T6SS potentiates <i>Vibrio cholerae</i> invasion of zebrafish intestines occupied by a commensal species .....	26
3.4 <i>Aeromonas</i> are expelled in frequent, sudden collapses from fish guts invaded by T6SS-expressing <i>V. cholerae</i> .....	28

Chapter	Page
3.5 Constitutively expressed T6SS alters the intestinal movements of larval zebrafish in an ACD-dependent manner.....	32
3.6 Materials and methods .....	36
Ethics statement .....	36
Gnotobiotic techniques .....	36
Bacterial strains and culture conditions .....	36
Culture-based quantification of bacterial populations .....	37
In vitro measurements of bacterial competition.....	38
Light sheet fluorescence microscopy.....	39
Sample handling and mounting for imaging.....	39
Imaging-based quantification of bacterial populations.....	40
Identification of population collapse events .....	40
Intestinal motility measurements .....	41
3.7 Discussion.....	41
IV. AUTOMATED HIGH-THROUGHPUT LIGHT-SHEET MICROSCOPY .....	45
4.1 Introduction.....	45
4.2 Instrument design, development, use, and limitations.....	48
Instrument design.....	48
Optical quality.....	51
Data collection capabilities .....	53
Neutrophils in larval zebrafish.....	54
Positioning accuracy .....	54

Chapter	Page
Neutrophil number and variance.....	55
4.3 Materials and methods.....	59
Hardware.....	59
Ethics statement.....	59
Zebrafish husbandry .....	59
Sample preparation .....	60
LPS treatment.....	60
Imaging procedure.....	61
Point spread function .....	62
Image-based neutrophil quantification .....	62
4.4 Discussion.....	63
 V. DISCUSSION AND FUTURE WORK.....	 66
5.1 Introduction.....	66
5.2 Immune deficient zebrafish and the type VI secretion system .....	67
5.3 A high-throughput closed-loop design and inflammation screening protocols.....	70
5.4 High-throughput visualization of immune cells .....	72
5.5 Summary and discussion.....	73
 REFERENCES CITED.....	 75

## LIST OF FIGURES

Figure	Page
1. Brightfield image of a larval zebrafish .....	4
2. Sample chamber of a light sheet microscope.....	10
3. Light sheet image of bacteria in a larval zebrafish gut .....	12
4. Differential interference contrast image of a larval zebrafish intestine.....	14
5. Genes of the type VI secretion system, sample images of a larval zebrafish and intestinal bacteria, and bacterial colonization abundances and competition ratios <i>in vitro</i> and <i>in vivo</i> .....	23
6. <i>In vitro</i> abundances of <i>Aeromonas</i> when mixed with <i>Vibrio</i> , schematic of protocol used to characterize bacterial interactions, histogram of <i>Aeromonas</i> abundances in the larval gut, and maximum intensity projections of <i>Aeromonas</i> after invasion by T6SS strains.....	29
7. Time series of <i>Aeromonas</i> when challenged by different strains of <i>Vibrio</i> and maximum intensity projections of <i>Aeromonas</i> invaded by T6SS+ <i>Vibrio</i> at 9.3, 10.7, and 16.3 hours after the start of imaging .....	31
8. DIC image of a larval zebrafish intestine, frequency and amplitude of periodic gut motion of larval zebrafish when germ-free or mono-associated with T6SS strains, <i>in vitro</i> killing rates of <i>Aeromonas</i> by T6SS+ and T6SS+ACD- strains, and histogram of <i>Aeromonas</i> abundances in the gut 24 hours after invasion by T6SS+ and T6SS+ACD- strains .....	34
9. Instrument design.....	49
10. Specimen positioning and image quality .....	52
11. Imaging neutrophils in larval zebrafish .....	56
12. Neutrophil counts after exposure to LPS .....	58
13. Gut motility amplitudes of MyD88 mutant zebrafish mono-associated with T6SS+ and T6SS- strains.....	69
14. Schematic for closed-loop high-throughput imaging .....	71



CHAPTER I  
MICROBES, HOSTS, PATHOGENS, AND THE IMMUNE SYSTEM

**1.1 Introduction**

Vertebrates are hosts to trillions of microorganisms, many of which compete and cooperate in the densely packed gut environment. This collection of microorganisms, both inside and outside the gut, is referred to as the microbiota. The human microbiota has been shown to play an important role in health and a variety of diseases (Consortium, 2012; Rajilić-Stojanović et al., 2013). By better understanding how microbes interact with each other and with their hosts, we can gain insights into human health and how it might be modified by microbial symbionts.

Previous research on the microbiota has largely employed the use of fecal samples; by collecting fecal samples and using high-throughput 16S ribosomal RNA sequencing, researchers can obtain a snapshot of the microbes present in the intestine and the genes that are actively expressed in those bacterial communities (Abu-Ali et al., 2018; Bashiardes et al., 2016). However, sequencing cannot determine the spatial structure, or spatial and temporal dynamics, of the bacterial communities inhabiting the intestine. These aspects of the microbiota are essential for understanding ecological interactions between bacteria in the gut, for creating a more complete picture of host-microbe interactions, and for understanding how pathogens might invade and establish themselves in the intestinal environment.

In order to elucidate the spatial and temporal aspects of the vertebrate microbiota, we employ the use of light sheet fluorescence microscopy and larval zebrafish as a model

organism. This chapter will provide an introduction to the microbiota, model organisms, pathogenic invasion mechanisms, and the immune system. Chapter II describes light sheet fluorescent microscopy, including its function, current work in the field, and limitations. Chapter III describes work using light sheet fluorescence microscopy to study the role of a bacterial mechanism, the type VI secretion system, in invading an established bacterial community in the larval zebrafish intestine. Chapter IV describes an automated high-throughput light sheet fluorescence microscope designed and built in our lab. Chapter V focuses on future work and provides concluding remarks.

## 1.2 Model Organisms

Model organisms are widely used in science to study biological phenomena. Generally, model organisms are easy to breed and maintain, and many have genes and genetic diseases similar to those found in humans. The use of animals to study biology dates back to ancient Greece (Cohen and Loew, 1984) and has led to scientific advances including the chromosomal theory of inheritance (Benson, 2001), the development of a diphtheria antitoxin (Haas, 2001), methods of tissue and organ transplants (Streilein, 1965), and much more. Common model organisms include yeast (Botstein et al., 1997), mice (Perlman, 2016), fruit flies (Jennings, 2011), *C. elegans* (Riddle et al., 1997), and zebrafish (Dooley and Zon, 2000).

For studies of the microbiota, each common model organism has advantages and disadvantages. *C. elegans* is an excellent model for gut microbiota research because it is simple and genetically tractable; its use has been proven in studying the direct and indirect effects of micronutrients via the gut microbiota (Yilmaz and Walhout, 2014),

studying community assembly in many nearly identical individuals (Vega and Gore, 2017), and much more. Similarly, *Drosophila melanogaster* is a well-established model for studying the microbiota because it is easy to culture and manipulate; *D. melanogaster* has also been used in studies of microbial community assembly (Adair et al., 2018), as well as studies of microbiota-dependent gene regulation (Dobson et al., 2016), gut microbiota community structure (Martinson et al., 2017), and more. However, *C. elegans* and *D. melanogaster* are relatively dissimilar from humans when compared to other common model organisms, and their gut microbiotas tend to be highly dependent on their food and environment, suggesting that they allow fewer insights into host-specific microbe selection. Mice, on the other hand, are anatomically, genetically, and physiologically much more similar to humans, and can even be colonized with human gut microbes (Nguyen et al., 2015). However, mice are more expensive to house and have much longer generation times than other small model organisms. Moreover, mice are not transparent under light microscopy, making it very difficult to examine *in vivo* spatial structure and dynamics of gut microbial communities.

For our work on host-microbe interactions, we have chosen to use larval zebrafish as a model organism. Larval zebrafish are an appealing model organism for many reasons: they have a genetic structure and mutant phenotypes similar to those of humans (Dooley and Zon, 2000), they reproduce rapidly and in large numbers (Howe et al., 2013), they can be raised free of microbes (Milligan-Myhre et al., 2011), and they are relatively transparent in their embryonic and larval stages. This transparency allows in-depth microscopy studies to probe features such as development (Tomer et al., 2012; Weber et al., 2017), host-microbe interactions (Hill et al., 2016), and microbial dynamics

within the intestine (Logan et al., 2018; Wiles et al., 2016). Furthermore, the dynamics of unlabeled, semi-transparent intestinal tissue in larval zebrafish can be imaged using differential interference contrast microscopy (DICM) (Baker et al., 2015). Figure 1.1 shows a larval zebrafish at 5 days post-fertilization (dpf).



**Figure 1.1.** Brightfield image of a 5 dpf larval zebrafish; the gut has been colored with phenol red dye via oral gavage for easy identification. This fish is an example of the model organisms used in our host-microbiome research. Scale bar: 1 mm.

By inoculating larval zebrafish with fluorescently labeled bacteria, we can probe bacterial dynamics and host-microbe interactions inside of these live hosts. Furthermore, zebrafish can be genetically modified to express fluorescent proteins in their cells; this allows image-based observations of their responses to various stimuli, such as select bacterial strains or chemical compounds. Several sections of this dissertation will explore

the dynamics of fluorescently labeled bacteria in the intestine and hosts' responses to those bacteria.

### **1.3 Pathogens, colonization resistance, and microbial competition mechanisms**

As previously mentioned, microbes residing in vertebrate intestinal tracts play an important role in health and disease. It has been established that these communities of bacteria can help defend their vertebrate counterparts from invading pathogens; this action is often called “colonization resistance” (Buffie et al., 2015; Spees et al., 2013; van der Waaij et al., 1971; Young, 2017). In spite of this feature, many pathogens can still enter the environment and establish themselves in hosts' intestines. Understanding how certain pathogens overcome colonization resistance may therefore help us design therapies to prevent infection by pathogens, either by modifying our own microbiomes or by targeting certain pathogenic mechanisms. One such mechanism, the type VI secretion system (T6SS), and its effects on both the host and resident gut microbial communities, is explored in detail in Chapter III.

The T6SS is a syringe-like bacterial apparatus present in many microbes, including several strains found in the human microbiota (Verster et al., 2017). The T6SS is used primarily as a contact-mediated weapon against neighboring cells; nearby cells are “stabbed” and toxic proteins are injected to cause cell death (Ho et al., 2014; Russell et al., 2014a). While most work has focused on the role of the T6SS in competition with other bacterial strains, it has also been shown to impact eukaryotic hosts (Hachani et al., 2016; Ma and Mekalanos, 2010). In our work, the T6SS of a human pathogen, *Vibrio*

*cholerae*, is modulated to determine its affects on both the host and competing bacterial strains in the intestine.

*Vibrio cholerae*, the bacteria that causes cholera in humans, is an important pathogen to study in its own right. Cholera is easily contracted through contaminated food or water, and the lifecycle of cholera can lead to major outbreaks; cholera multiplies in the intestine and causes watery diarrhea, which returns the microbe to the water supply in even greater numbers. Cholera can quickly become fatal; death can result within 48 hours if cholera is left untreated (Orata et al., 2014). Cholera outbreaks were documented as early as the 5<sup>th</sup> century BC (Harris et al., 2012), and recent outbreaks in Haiti and Africa have highlighted its importance as a modern global pathogen (Orata et al., 2014). The seventh cholera pandemic began in 1961 in Indonesia and continues today; an estimated 3-5 million people are affected each year and approximately 120,000 die (Zuckerman et al., 2007).

Our work probes the impact of the *V. cholerae* T6SS on its ability to invade and establish itself in hosts' intestines. The T6SS is only one small part of *V. cholerae* pathogenesis, but a complete understanding of the strategies and abilities of deadly pathogens is an important aspect of combating and eventually eradicating them.

#### **1.4 The immune system, neutrophils, and inflammation**

In studying pathogens, invasion, and host-microbe interactions, focusing on the host can often be as telling as focusing on the microbes. In our work, the immune system has become an important host feature to study, both in light of bacterial interactions and in its own right. Lines of genetically modified zebrafish have been developed to study the immune system, including lines for visualizing neutrophils (Renshaw et al., 2006),

macrophages (Ellett et al., 2011), and tumor necrosis factor alpha (tnfa) (Nguyen-Chi et al.). Neutrophils are highly motile cells that make up part of the innate immune system; these cells can travel to damaged or infected sites and kill unwanted microbes (Mayadas et al., 2014). Macrophages are another important cell type of the innate immune system that is recruited to injury sites after neutrophils have responded (Prame Kumar et al., 2018). Tnfa is a central inflammatory cell signaling protein, which marks certain types of macrophages and can be a good indicator of many inflammatory responses (Nguyen-Chi et al.; Parameswaran and Patial, 2010). By visualizing these parts of the immune system, we can learn about zebrafish immune responses to gut bacteria, specific chemical compounds, and other stressors. Furthermore, developing a streamlined protocol for high-throughput inflammation screening in transgenic zebrafish could open the door to myriad future studies. Current and future work on these topics is discussed in Chapter V.

## **1.5 Discussion**

The microbiota is an important area of study because of its role in health and disease. Zebrafish are an excellent candidate for imaging studies of the microbiota because they are transparent in their larval stage, they reproduce quickly, and they are genetically similar to humans, among many other appealing characteristics. The microbiota also plays an important role in resisting pathogenic invasion, and understanding what mechanisms pathogens use to overcome this resistance could provide insights into preventing certain diseases, including cholera. The immune system is an aspect of host-microbe interactions in the gut that warrants future study, and exploring

this facet of the host-microbe ecosystem will further elucidate the intestinal microbiota's role in health, disease, and pathogenic interactions.

In order to use zebrafish as a model organism for visualizing the microbiota and the immune system, advanced microscopy techniques are necessary. The next chapter will describe light sheet fluorescence microscopy, which can be used to image the entire larval zebrafish intestine with single-bacteria resolution, minimal phototoxicity, and a wide field of view.

The work described in this dissertation is based largely on co-authored material. Chapter III contains published co-authored material with contributions from Jacob Thomas, Jinyuan Yan, Ryan P. Baker, Drew S. Shields, Joao B. Xavier, Brian K. Hammer, and Raghuveer Parthasarathy. Chapter IV contains soon-to-be published material with contributions from Christopher Dudley, Ryan P. Baker, Michael J. Taormina, Edouard A. Hay, and Raghuveer Parthasarathy.



## CHAPTER II

### LIGHT SHEET FLUORESCENCE MICROSCOPY

#### 2.1 Introduction

We image intestinal microbial populations and fluorescently labeled tissues in larval zebrafish using a form of three-dimensional microscopy called light sheet fluorescence microscopy (LSFM). In LSFM, a thin sheet of laser light is aligned perpendicular to and in the focal plane of an imaging objective. This sheet of light excites fluorophores in roughly micron-thick slices of a sample (in our experiments, a live larval zebrafish), which is positioned in the path of the sheet. The sample can be moved through the sheet to create a stack of two-dimensional images that together form a three-dimensional image. This method has many advantages over other forms of microscopy, including low phototoxicity, high resolution, high speed, and a wide field of view (Huisken, 2012; Keller et al., 2008, 2014; Power and Huisken, 2017; Santi, 2011). The light sheet fluorescence microscopes used in this work and described in the following chapters were home-built based on the design of Keller et al. (2008). Figure 2.1 shows the sample chamber of one of our home-built light sheet fluorescence microscopes with six larval zebrafish mounted for imaging, each held in agar gel protruding from the end of a glass capillary. These microscopes can image the entire larval zebrafish intestine with micron-scale resolution, and low phototoxicity allows for many-hour live imaging of intestinal bacterial populations over time (Jemielita et al., 2014; Logan et al., 2018; Taormina et al., 2012; Wiles et al., 2016).

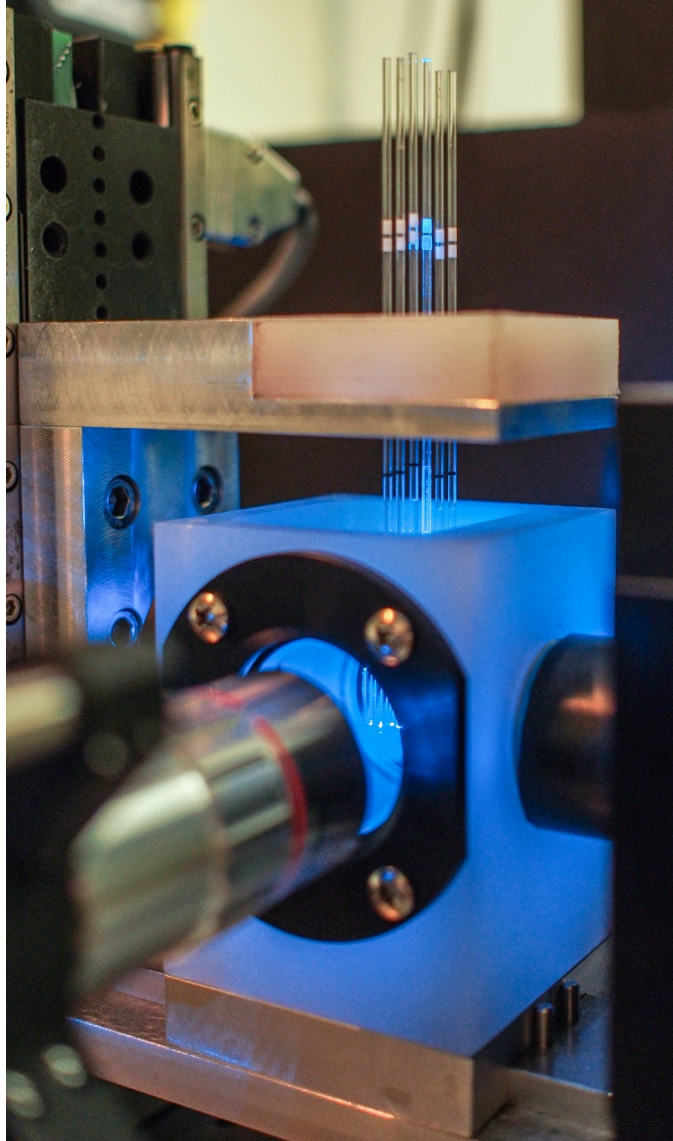


**Figure 2.1.** The sample chamber of one of the home-built light sheet microscopes in the Parthasarathy lab. A sheet of laser light enters the chamber from the objective on the left and hits one of six larval zebrafish mounted for imaging. The imaging objective is partially visible on the right, perpendicular to the sheet.

## 2.2 Current work in light sheet fluorescence microscopy

Light sheet microscopy was first developed in 1902 using scattered light (Siedentopf and Zsigmondy, 1902), and the first light sheet fluorescence was reported in 1993 (Voie et al., 1993). Beginning in the early 2000s, LSFM became immensely popular as a tool of visualizing biological phenomena. Uses have ranged from 3D imaging of embryonic development in zebrafish, (Keller et al., 2008), mice (McDole et al., 2018; Udan et al., 2014), and fruit flies (Khairy et al., 2015), to mapping of neural activity (Keller and Ahrens, 2015), to elucidating whole cardiac and brain structure (Fei et al., 2016; Stefaniuk et al., 2016), and much more. Most recently, improvements to resolution and optical capabilities have come to the forefront, including developments such as structured illumination (Chang et al., 2017; Chen et al., 2014), two-photon excitation (Truong et al., 2011), and adaptive optics (Liu et al., 2018).

One of the focuses of the Parthasarathy lab is to use LSFM as a tool to study the intestinal microbiota and host-microbe interactions. As discussed in section 1.2, larval zebrafish can be inoculated with bacteria engineered to express fluorescent proteins, and these communities can be monitored and imaged in 3D over long periods of time using LSFM. The work in the following chapters would not have been possible without significant work from previous members of the Parthasarathy lab, who built the microscopes used in this research and developed an imaging and analysis pipeline for efficiently studying bacterial communities in larval zebrafish intestines.

Both light sheet microscopes built in the Parthasarathy lab follow the design of Keller et. al (2008), and the first is described in detail in Taormina et. al (2012). At the time the Parthasarathy lab began using LSFM, no commercial light sheet microscopes

were available for purchase, necessitating a home-built instrument. Interestingly, several companies now offer commercial instruments, including Applied Scientific Instruments and Zeiss. Home-building a light sheet fluorescence microscope, while time consuming, allowed customizations based on the needs of the lab, including optimization of sheet thickness and magnification and, importantly, a sample chamber capable of holding multiple specimens, which have proven very useful for imaging bacterial communities in larval zebrafish intestines.

Using this microscope, aspects of bacterial growth can be measured inside of a live host, including spatial and temporal features that were previously impossible to explore. Particularly, the entire bacterial population inside of the fish intestine could be quantified as it grew from individuals to tens of thousands over several hours, and interesting features, such as bacterial distribution along the gut and the growth of aggregates versus individuals, could be studied in depth for the first time (Jemielita et al., 2014).

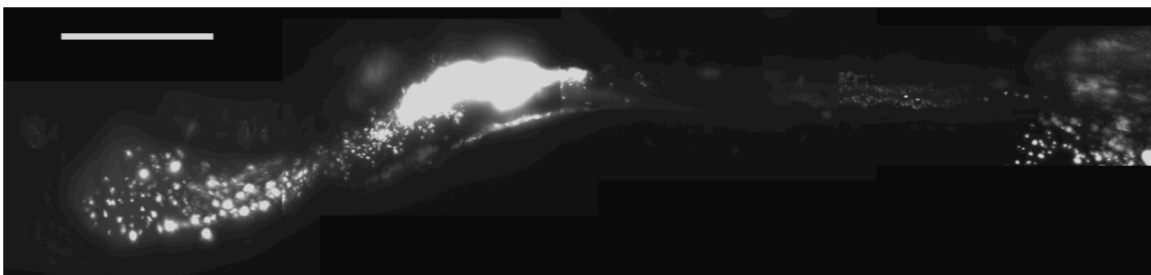


**Figure 2.2.** A single-plane light sheet image of a fluorescently labeled bacterial community inside of a larval zebrafish intestine. This image was acquired using the home-built microscope shown in figure 2.1. The anterior of the zebrafish is to the left, and the vent can be seen on the far

right. Individual bacteria and small clusters are visible in the bulb on the left, and a bright mid-gut clump can be seen in the center. Scale bar: 200 um.

To further improve the capabilities of the lab's light sheet fluorescence microscope, a differential interference contrast microscopy (DICM) path was added in 2015 (Baker et al., 2015). DICM complements LSFM by allowing imaging of unlabeled, semi-transparent tissue with high contrast and optical sectioning. LSFM inherently requires the use of fluorescently labeled cells, and DICM can give important context to LSFM images by revealing the surrounding tissues and their dynamics. For example, DICM can image the transparent tissue surrounding the intestine and measure its motility over a period of several minutes, which can be quantified using techniques developed in the Parthasarathy lab (Ganz et al., 2018). Notably, none of the currently available commercial light sheet fluorescence microscopes have DIC capabilities. The Parthasarathy lab's combined LSFM/DICM, and an established analysis pipeline for the resulting data, was particularly important for the work described in Chapter III of this dissertation. An example of DICM is shown in figure 2.2.

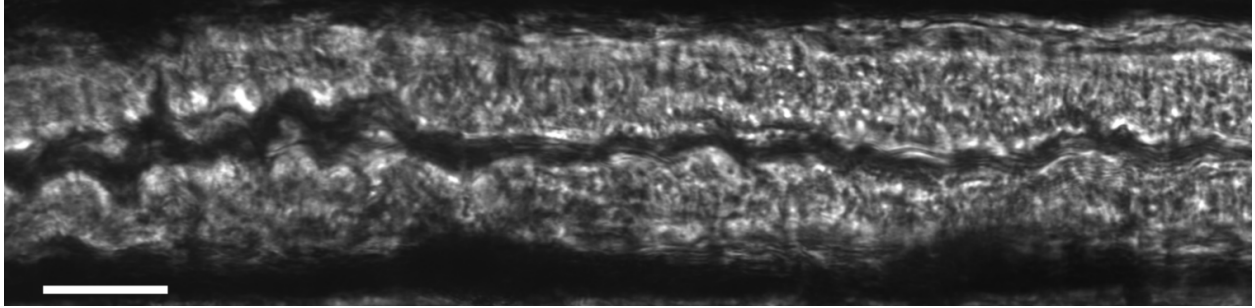


**Figure 2.2.** A differential interference contrast image of a portion of a larval zebrafish intestine. The dark horizontal section in the center of the image is the lumen, and the lighter surrounding area is the epithelial tissue. Scale bar: 50  $\mu\text{m}$ .

These developments in microscopy allowed more in-depth studies of multispecies bacterial dynamics in the intestine, and the impact of the gut environment on these communities could be observed using a combination of LSM and DICM. In particular, researchers in the Parthasarathy and Guillemin labs were able to observe, quantify, and understand an interesting example of competition between two bacterial species native to the zebrafish gut, uncovering distinct spatiotemporal patterns of the bacterial populations that interacted with intestinal motility to control apparent competition (Wiles et al., 2016). The two competing species, *Aeromonas veronii* and *Vibrio cholerae*, both colonize to high numbers if alone. However, if *Aeromonas* is allowed to colonize and is then followed by *Vibrio*, its population decreases and becomes highly variable. Light sheet fluorescence imaging showed sudden expulsions of *Aeromonas*, with features that fit a model of logistic growth punctuated with stochastic collapses. The two species exhibited different spatial features, with *Aeromonas* populations largely clumping in the

mid-gut and *Vibrio* populations being made up of motile, planktonic individuals residing mostly in the anterior region of the gut. These differences in biogeography and community architecture led to the two species responding differently to peristalsis. When peristalsis was reduced using larval zebrafish with a mutation in the *ret* gene locus, the competition between the two bacterial species was eliminated. This study highlighted the importance of understanding the spatial and temporal dynamics of the intestinal microbiota and also emphasized that *in vivo* monitoring of bacterial communities reveals interactions that can be completely absent *in vitro*. This work paved the way for many future studies in the lab, including the work described in Chapter III.

A second light sheet fluorescence microscope was constructed primarily by graduate student and postdoctoral fellow Michael Taormina beginning in 2014. This microscope, while also based on the design of Keller et. al (2008), integrated upgrades not present in the original UO light sheet fluorescence microscope, most notably the use of fiber optic cables for excitation illumination. This microscope has been integrated with the automated, high-throughput design described in Chapter IV and is presently located in the University of Oregon Biological Imaging Core Facility.

### **2.3 Limitations of current light sheet fluorescence microscopes**

As discussed in the previous section, LSFM has undergone a surge in popularity over the last ten years, with major developments in design, uses, and optical capabilities. However, current light sheet microscopes face significant limitations due to low throughput and tedious sample handling and preparation. Most current light sheet fluorescence microscopes can hold only one specimen at a time; a few, including those

built by our group, can hold up to six specimens for sequential imaging. Furthermore, sample preparation is almost always done manually and involves tedious, labor-intensive steps, making data collection time consuming and relatively low-throughput. This is a major limitation for LSFM, because large variation in many biological characteristics of interest prevents patterns from emerging unless datasets are sufficiently large. One automated light sheet microscope has been reported in the literature so far, although its throughput is unclear (Gualda et al., 2015). Chapter III describes a new, automated high-throughput light sheet microscope developed in our lab to combat these issues.

## 2.4 Discussion

Light sheet fluorescence microscopy is a powerful tool for studying a wide range of biological phenomena, and its popularity in recent years has led to rapid advancements in design, optical capabilities, and throughput. The Parthasarathy lab has pioneered the use of LSFM to study *in vivo* bacterial dynamics using larval zebrafish as a model organism, which has led to profound insights into spatiotemporal structure and host interactions in intestinal microbial communities. The next chapter will explore work using LSFM to study another aspect of the intestinal microbiota: how it is impacted by invading pathogens, a mechanism that pathogens might use to invade it, and the effect of host-pathogen interactions on an established bacterial community.



## CHAPTER III

### THE VIBRIO CHOLERAE TYPE VI SECRETION SYSTEM CAN MODULATE HOST INTESTINAL MECHANICS TO DISPLACE GUT BACTERIAL SYMBIONTS

This chapter contains previously published co-authored material; it has been adapted from S. L. Logan, J. Thomas, J. Yan., R. P. Baker, D. S. Shields, J. B. Xavier, B. K. Hammer, and R. Parthasarathy, “The *Vibrio cholerae* Type VI Secretion System Can Modulate Host Intestinal Mechanics to Displace Gut Bacterial Symbionts.” *Proc. Natl. Acad. Sci.* **115**: E3779-E3787 (2018). In this work, I contributed to designing the research, performing the research, analyzing the data, and writing the paper.

#### **3.1 Introduction: *Vibrio cholerae* and the type VI secretion system**

The consortium of microbes that make up the human microbiome plays important roles in health and disease (Consortium, 2012; Rajilić-Stojanović et al., 2013). In the gastrointestinal tract, where most animal-associated microbiota reside and where the potential interface of interspecies contact is large, commensal microbes prevent colonization by pathogens, a function termed colonization resistance (Buffie et al., 2015; Spees et al., 2013; van der Waaij et al., 1971). Colonization resistance can, however, be thwarted by pathogens as the first stage of infectious disease; the mechanisms used in this inter-species competition remain unclear. By understanding how pathogens interact with commensal communities, we may more rationally design future therapies focused on targeting the pathogens themselves, or on engineering the host microbiome to better resist disruption. Uncovering these mechanisms, however, has proven challenging due to the

difficulties of *in situ* monitoring of intestinal microbial populations and precise control of expression of pathogenic phenotypes.

We consider the transient human pathogen *Vibrio cholerae*, which can successfully colonize the human gut following ingestion of contaminated food or water. There, it causes diarrhea that may return the microbe to aquatic reservoirs in even larger numbers, leading to outbreaks. Cholera diarrhea causes severe dehydration and can be fatal if untreated. Recent epidemics in Haiti and Africa highlight that *V. cholerae* remains a major global problem and underscore that a better mechanistic understanding of the lifestyle of this microbe can help control future cholera outbreaks and infection (Barzilay et al., 2013).

*V. cholerae* can form biofilms on chitinous substrates such as the exoskeleton of crustaceans (Silva and Benitez, 2016) and can colonize the gut of birds (Laviad -Shitrit et al., 2017) and fish (Halpern and Izhaki, 2017), which may promote transmission in aquatic environments. Within a human host, a complex set of signaling systems and external cues regulate colonization and disease factors: biofilm formation, chemotactic-guided flagella, toxin-coregulated pili, several adhesins, and cell shape features to ensure the microbe's access to the intestinal surface (Almagro-Moreno et al., 2015; Bartlett et al., 2017). Toxigenic isolates that carry the CTXphi prophage secrete the potent cholera toxin, which triggers rapid fluid loss and massive diarrhea. While cholera toxin itself serves as a competition factor by promoting dispersal of gut commensals, less is understood regarding additional factors that enable *V. cholerae* cells entering the gut to compete with the daunting assemblage of gut microbiota they encounter. Recent human studies show that cholera diarrhea disturbs the composition of the commensal microbiota

(David et al., 2015) and studies in humans combined with mammalian animal models suggest that the microbiome composition affects how the host recovers from the disease (Hsiao et al., 2014).

Here, we sought to discover how *V. cholerae* may overcome resident commensals to invade a host intestine. We focused on the role of the type VI secretion system (T6SS), a syringe-like protein apparatus present in nearly 25% of all Gram-negative bacteria that inflicts damage on target cells by direct contact. The T6SS spike and inner tube pierce adjacent cells and deliver multiple “effector” molecules that can be deadly to eukaryotic cells, as well as bacteria that lack immunity protein (Hachani et al., 2016; Ho et al., 2014; Russell et al., 2014b). T6 activity in non-toxigenic, environmental isolates and toxigenic, CTXphi isolates derived from clinical sources are controlled by diverse regulatory systems and external cues (Bernardy et al., 2016; Joshi et al., 2017). More recently, a role for T6-mediated microbe-microbe interactions within the mouse gut has been demonstrated for *Shigella* and *Salmonella* infection (Anderson et al., 2017; Sana et al., 2016). Commensal *Bacteroides* can use their T6SS to compete with other bacteria to maintain their presence in the mouse gut (Chatzidaki-Livanis et al., 2016; Wexler et al., 2016). T6SS genes have been detected in the human gut microbiome as well (Coyne et al., 2014; Russell et al., 2014a). All of this evidence suggests that T6SSs require more attention for their role in the initiation and development of cholera, and also in mediating microbe-microbe and microbe-host interactions in the gut microbiome.

Investigating the potential role of the *V. cholerae* T6SS in intestinal invasion is challenging in humans, and even in mammalian model organisms, due to the complexity of colonization and infection processes and the severe difficulty of *in vivo* imaging. By

contrast, zebrafish are a powerful laboratory model for the direct observation and experimental control of microbiome interactions. Germ-free and gnotobiotic protocols allow precise control of intestinal microbial composition (Milligan-Myhre et al., 2011). Zebrafish are relatively transparent at larval stages. Thus, light sheet fluorescence microscopy (Jemielita et al., 2014; Keller, 2013; Keller et al., 2008) can be used to capture detailed three-dimensional images of fluorescently-labeled bacteria, spanning the entire gut, over many hours, to monitor both sudden and longer-term transitions in bacterial populations (Wiles et al., 2016), and differential interference contrast microscopy can capture the dynamics of unlabeled intestinal tissue in the same animal (Baker et al., 2015).

Mammalian models for *V. cholerae* infection have revealed modest contributions of the T6SS in the infant rabbit (Fu et al., 2013), and fluid accumulation in the infant mouse (Ma and Mekalanos, 2010). However, these organisms, unlike fish (Zhao et al., 2018) or humans, are not natural *V. cholerae* hosts (Lescak and Milligan-Myhre, 2017). Recent studies have demonstrated the utility of the zebrafish as a model for cholera intestinal colonization, pathogenesis, and transmission (Borgeaud et al., 2015), revealing for example that fish colonization is independent of cholera toxin (Runft et al., 2014). Together, these features make the zebrafish an ideal model for studying the dynamics of vertebrate gut colonization by *Vibrio cholerae*, and specifically the role of its T6SS.

In this study, we combined microbial genetics, *in vitro* experiments and quantitative *in vivo* imaging in zebrafish to determine the role of the T6SS of *V. cholerae* in gut colonization. We exploited the known regulation pathways of T6SS (Mitchell et al., 2017; Watve et al., 2015; Zheng et al., 2011) to genetically manipulate the human-

pathogenic *V. cholerae* wild type El Tor strain C6706 to constitutively express functional, defective, or altered T6SS machinery, as well as generating strains lacking T6SS immunity. We then imaged at high resolution the invasion by *V. cholerae* of zebrafish intestines that were previously colonized by a zebrafish-commensal *Aeromonas* species. Our experiments show a strongly T6SS-dependent displacement of the resident bacteria. The displacement took the form of sudden collapses in *Aeromonas* populations via ejections of aggregated bacteria from the gut, similar to the collapses previously reported for *Aeromonas* when challenged by a fish-commensal species of the genus *Vibrio* (Wiles *et al.*, 2016). We found that the expression by *V. cholerae* of a functional T6SS induced a large increase in the amplitude of the peristaltic movements in the host intestine. Deletion of the actin cross-linking domain (ACD) of one of the T6SS spike proteins returned zebrafish gut activity to normal and eliminated *V. cholerae*'s ability to expel the commensal *Aeromonas* from the gut, without affecting its ability to kill *Aeromonas* cells *in vitro*.

To the best of our knowledge, ours is the first observation that the bacterial T6SS can induce organ-level physiological changes in an animal host that displace resident microbiota and enable colonization, in an ACD-dependent manner. These findings expand the array of known molecular mechanisms by which pathogens can leverage host-microbe interactions to redefine microbial community composition, and also suggest that the T6SS could be rationally manipulated to deliberately engineer the human microbiome.

### **3.2 Human-derived *Vibrio cholerae* colonizes the larval zebrafish intestine but exhibits weak intra-species T6SS-mediated killing *in vivo***

A streptomycin resistant mutant of patient-derived El Tor biotype C6706 served as a "wild type" strain (denoted T6SS<sup>WT</sup>) as it is proficient at T6-mediated bacterial killing (Pukatzki et al., 2006; Zheng et al., 2011). T6SS and immunity genes are well characterized in this strain, allowing us to construct variants that differed in T6SS expression, immunity, and functionality (Fig. 1A). A strain constitutive for T6SS expression, termed T6SS<sup>+</sup>, was previously constructed by replacement of the native *qstR* promoter, and a T6SS<sup>-</sup> derivative of this strain was constructed by deletion of the *vasK* gene ( $\Delta vasK$ ) (Thelin and Taylor, 1996). Further deletion of three T6 immunity genes (*tsiVI-3*) generated a T6SS<sup>-</sup> Imm<sup>-</sup> strain. Each strain was labelled fluorescently either with a chromosomally-introduced teal or orange fluorescent protein to enable microscopy (Thelin and Taylor, 1996).

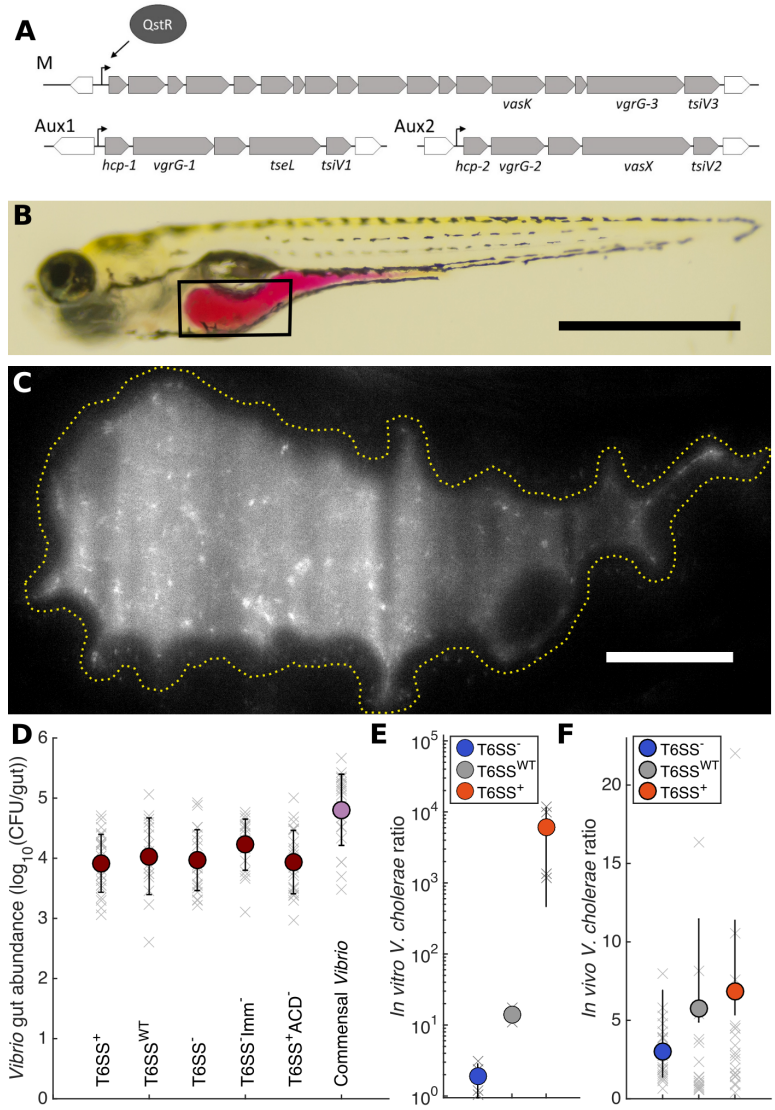


**Figure 3.1** (A) Genes of the *V. cholerae* C6706 Type VI secretion system. T6SS genes are primarily organized in three operons that are transcriptionally activated through the regulator QstR. The main cluster (M) encodes most of the T6SS structural genes while the major Hcp subunit is encoded on the auxiliary clusters Aux1 and Aux2. Each cluster terminates in genes encoding antibacterial effectors (TseL, VasX and VgrG-3) and their respective immunity proteins (TsiV1-3). Each cluster

also encodes proteins that form a spike at the apex of the apparatus, VgrG-1-3. Two of the three VgrG proteins are multifunctional: VgrG1 contains a C-terminal actin crosslinking domain (ACD), and VgrG-3 has a muramidase domain that serves as an antibacterial effector. (B) A larval zebrafish at 5 dpf with the intestine colored for illustration by orally gavaged phenol red dye. Scale bar: 1mm. (C) A light sheet fluorescence image of wild type *V. cholerae* expressing orange fluorescent protein in the larval zebrafish intestine. The region shown roughly corresponds to the box in (B), with the luminary boundary roughly indicated by the yellow dotted line. Individual motile bacteria are evident, as is the background autofluorescence of the gut lumen. See also Supplemental Movie 1. Scale bar: 50 $\mu$ m. (D) Abundance of *Vibrio* strains in the larval zebrafish intestine at 24 hours post-inoculation. All *V. cholerae* strains robustly colonize to approximately  $10^4$  bacteria per fish, roughly an order of magnitude lower than a commensal *Vibrio* species (rightmost data points). Measurements from individual fish at 6 dpf are shown in grey, averages are indicated by solid colored circles, and black error bars represent quartiles. (E) Ratios of *V. cholerae* strains in an *in vitro* competition assay. Each indicated strain was mixed 1:1 with T6SS<sup>-</sup> Imm<sup>-</sup> as a target, and spotted onto a nylon membrane on agar. Ratios were determined from CFU counts following 3h of incubation. The T6SS<sup>+</sup> strain exhibits a greater competitive advantage over the T6SS<sup>-</sup> Imm<sup>-</sup> strain. (F) Ratios of *V. cholerae* strains in the larval zebrafish intestine 24 hours after co-



inoculation. At 5 dpf, fish were co-inoculated with T6SS<sup>-</sup> Imm<sup>-</sup> as a target, and one of either wild type, T6SS<sup>-</sup>, or T6SS<sup>+</sup> strains. The T6SS<sup>+</sup> and wild type strains exhibit a slightly greater competitive advantage over the T6SS<sup>-</sup> Imm<sup>-</sup> strain compared to the T6SS<sup>-</sup> strain. In (E) and (F), measurements from individual fish are shown in grey, averages are indicated by solid circles, and quartiles are represented by black lines.

To determine whether the human-derived *V. cholerae* and its variants could colonize the larval zebrafish gut, we inoculated flasks housing germ-free larvae with a single bacterial strain at 5 days post-fertilization (dpf). We then dissected the gut at 6 dpf and determined intestinal bacterial abundance by serial plating and counting colony forming units (CFUs). For comparison, we also considered a previously examined zebrafish commensal bacterium ZWU0020 assigned to the genus *Vibrio* (McNally et al., 2017; Wiles et al., 2016). All *V. cholerae* strains examined could colonize the larval zebrafish intestine robustly to an abundance of approximately 10<sup>4</sup> CFU per gut, which is roughly one order of magnitude lower than the commensal *Vibrio* (Fig. 1B-D). Direct observation by light sheet fluorescence microscopy at 5 dpf showed that each strain of *V. cholerae* was abundant and highly motile in the intestinal lumen (Fig. 1C and Supplemental Movie 1).

We then asked whether we could detect signatures of T6SS-mediated intra-species competition *in vitro* and *in vivo*. For *in vitro* assays, we mixed two *V. cholerae* strains in liquid culture at a 1:1 ratio. One of these was always the T6SS<sup>-</sup> Imm<sup>-</sup> strain which, lacking immunity to T6SS, served as a "target" for inter-bacterial killing (Zheng

et al., 2011). We spotted the mix onto nylon membranes on agar plates, and allowed the microbes to interact in close proximity for 3 hours. We then quantified killing by measuring ratio of CFU counts for each pair of strains, which we distinguished by their fluorescent markers. T6SS<sup>-</sup> and T6SS<sup>WT</sup> strains were only slightly enhanced compared to the target; the T6SS<sup>+</sup> strain, however, dominated the mixture, indicating T6SS-mediated killing (Fig. 1E), consistent with prior *in vitro* work (Zheng et al., 2011). *In vivo*, we co-inoculated zebrafish flasks at 5 dpf with the orange-labelled T6SS<sup>-</sup> Imm<sup>-</sup> strain and one of either the teal-labelled wild type, T6SS<sup>-</sup> defective, or T6SS<sup>+</sup> constitutive strains at a 1:1 initial ratio. We determined their ratios in the fish at 6 dpf using gut dissection and then by plating, again differentiating the strains by their fluorescence (Fig. 1F). We found that the T6SS<sup>+</sup> and wild type strains, compared to the T6SS<sup>-</sup> strain, exhibited a small and variable competitive advantage over the T6SS<sup>-</sup> Imm<sup>-</sup> target strain, with abundance ratios of  $6.8 \pm 2.9$ ,  $5.8 \pm 2.6$ , and  $3.0 \pm 0.4$  for challenge by T6SS<sup>+</sup>, T6SS<sup>WT</sup>, and T6SS<sup>-</sup>, respectively (mean  $\pm$  s.e.m.). The *in vivo* killing rate by T6SS competent cells was only roughly a factor of 2 higher for strains with functional T6SS compared to strains without the functional T6SS (Fig. 1F); this is far less dramatic than the *in vitro* killing of *V. cholerae* by other *V. cholerae* (Fig. 1E).

### **3.3 Constitutive expression of the T6SS potentiates *Vibrio cholerae* invasion of zebrafish intestines occupied by a commensal species**

Next, we addressed the key question of whether the T6SS can affect the ability to invade an established, commensal intestinal microbial community. We used as our target species *Aeromonas veronii* strain ZOR0001, hereafter referred to as *Aeromonas*, a Gram-negative bacterium native to and commonly found in the zebrafish intestine (Rolig et al.,

2015). Prior work has shown that this strain can robustly mono-colonize germ-free larval zebrafish at  $10^3$ - $10^5$  bacteria per gut (Jemielita et al., 2014; McNally et al., 2017). *Aeromonas* forms dense bacterial aggregates *in vivo* (Jemielita et al., 2014), and can be invaded by the fish-commensal *Vibrio* sp. ZWU0020 (Wiles et al., 2016).

We first determined whether *Aeromonas* was susceptible to T6-mediated killing by *V. cholerae* *in vitro*. We mixed *Aeromonas* and *V. cholerae* strains in liquid culture and spotted them onto nylon membranes as in the previously described *in vitro* experiments. We then quantified killing by measuring *Aeromonas* CFU counts before and after the membrane incubation. *Aeromonas* CFU counts when mixed with T6SS<sup>-</sup> *V. cholerae* were indistinguishable from those of a control mix of *Aeromonas* with *Aeromonas* (Fig. 2A). Wild type *V. cholerae*, and particularly the T6SS<sup>+</sup> strain, decreased *Aeromonas* CFU counts significantly, indicating high inter-species killing rates (Fig. 2A), consistent with prior *in vitro* results with an *Escherichia coli* target (Bernardy et al., 2016).

To determine the role of the T6SS *in vivo*, we monocolonized zebrafish by inoculating flasks containing germ-free larvae with *Aeromonas* at 4 dpf, and then inoculated with one of the *V. cholerae* strains at 5 dpf (Fig. 2B,  $N \sim 30$  animals per *V. cholerae* strain). Gut dissection and serial plating at 6 dpf revealed dramatic differences in the *Aeromonas* abundance depending on the T6SS of the invading strain. *Aeromonas* challenged by T6SS<sup>-</sup> or T6SS<sup>-</sup> Imm<sup>-</sup> *V. cholerae* persisted in the gut at approximately 1000 CFU per fish on average (Fig. 2C, first and second panels). *Aeromonas* challenged by the T6SS<sup>+</sup> *V. cholerae*, however, fell to single-digit numbers, with zero detectable *Aeromonas* in over 50% of fish (Fig. 2C, bottom panel). *Aeromonas* challenged by the

wild type *V. cholerae* showed intermediate numbers between the T6SS<sup>-</sup>-challenged and the T6SS<sup>+</sup>-challenged strains (Fig. 2C, third panel). Live imaging 24 hours after the *V. cholerae* inoculation demonstrates the differential impacts on the resident *Aeromonas*, with large populations consisting of dense clusters and discrete individuals in the gut of larvae challenged by T6SS<sup>-</sup> *V. cholerae* (Fig. 2D), and few *Aeromonas* remaining in the gut of larvae challenged by T6SS<sup>+</sup> *V. cholerae* (Fig. 2E). Each of the invading *V. cholerae* strains was present at 6 dpf at approximately 10<sup>4</sup> CFU/gut.

### **3.4 *Aeromonas* are expelled in frequent sudden collapses from fish guts invaded by T6SS-expressing *V. cholerae***

To better characterize the strong T6SS-mediated effect of *V. cholerae* on gut-resident *Aeromonas*, we monitored bacterial population dynamics over 12-17 hour durations using light sheet fluorescence microscopy, capturing a three-dimensional image spanning the entire larval intestine every 20 minutes. We used the same inoculation protocol and began live imaging 8 hours after *V. cholerae* inoculation.

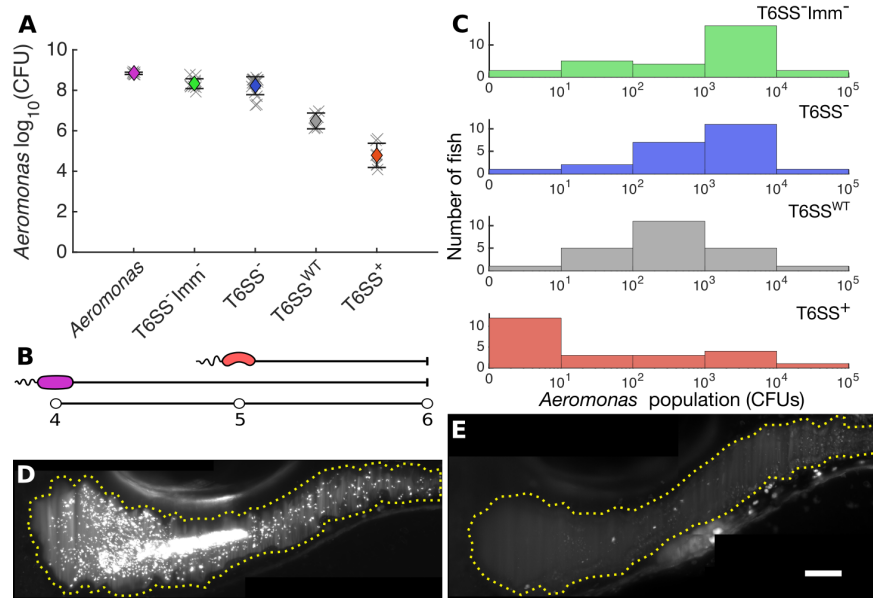


**Figure 3.2** (A) *In vitro* abundances of *Aeromonas* when mixed with *Vibrio cholerae* strains, determined from spotting liquid-cultured pairs of strains onto agar-supported membranes, 3h after mixing. (B) Schematic diagram of the protocol used to characterize *Aeromonas*–*Vibrio* interactions *in vivo*. *Aeromonas* (purple) is allowed to colonize at 4 dpf followed by inoculation of *V. cholerae* (red) strains into the surrounding water at 5 dpf. Imaging and/or dissections and serial plating occur at 6 dpf. (C) Histogram of *Aeromonas* abundances in the larval gut 24 hours after potential invasion by *V. cholerae* strains. The peak abundances are roughly 10<sup>3</sup> CFU/gut when *Aeromonas* is followed by T6SS<sup>-</sup> Imm<sup>-</sup> and T6SS<sup>-</sup>, 10<sup>2</sup> when followed by wild type, and 0 when followed by T6SS<sup>+</sup>. (D, E) Maximum intensity projections of a 3D light sheet image stack of *Aeromonas* in the larval gut 24 hours after invasion by T6SS<sup>-</sup> Imm<sup>-</sup> (D)

and T6SS<sup>+</sup> *V. cholerae* (E) with the boundaries of the gut lumen roughly indicated by yellow dotted lines. Scale bar: 50  $\mu\text{m}$ .

We had shown in previous work that *Aeromonas* populations residing the zebrafish intestine can be punctuated by occasional large collapses corresponding to ejection from the gut. In fish mono-colonized with *Aeromonas*, these collapses occurred at a mean rate of  $p_c = 0.04 \pm 0.02 \text{ hr}^{-1}$ , but in fish invaded by the commensal *Vibrio* ZWU0020 the rate of collapse increased to  $p_c = 0.07 \pm 0.02 \text{ hr}^{-1}$  (Wiles et al., 2016). Here, as in prior work, we defined a collapse as a population drop of at least a factor of ten in one 20-minute time interval, together with at least a factor of two drop relative to the original population at the subsequent time step. The *Aeromonas* population was strikingly stable when invaded by the T6SS<sup>-</sup> strains: we observed zero collapses during the entire 58.0 and 70.3 hour total imaging times for T6SS<sup>-</sup> ( $N = 5$  fish) and T6SS<sup>-</sup> Imm<sup>-</sup> ( $N = 6$  fish) *V. cholerae* challenges, respectively (Fig. 3A, first two panels). Challenge by the wild type *V. cholerae* resulted in two population collapses in 72.7 hours corresponding to a collapse rate  $p_c = 0.03 \pm 0.02 \text{ hr}^{-1}$  (Fig. 3A, third panel,  $N = 6$  fish). Challenge by T6SS<sup>+</sup> *V. cholerae* gave rise to large and frequent collapses, totaling 8 in 64.3 hours (Fig. 3A, last panel,  $N = 5$  fish), corresponding to a collapse rate  $p_c = 0.12 \pm 0.04 \text{ hr}^{-1}$ , nearly twice as large as that induced by the fish-commensal *Vibrio* ZWU0020 (Wiles et al., 2016) (Fig. 3B-D).

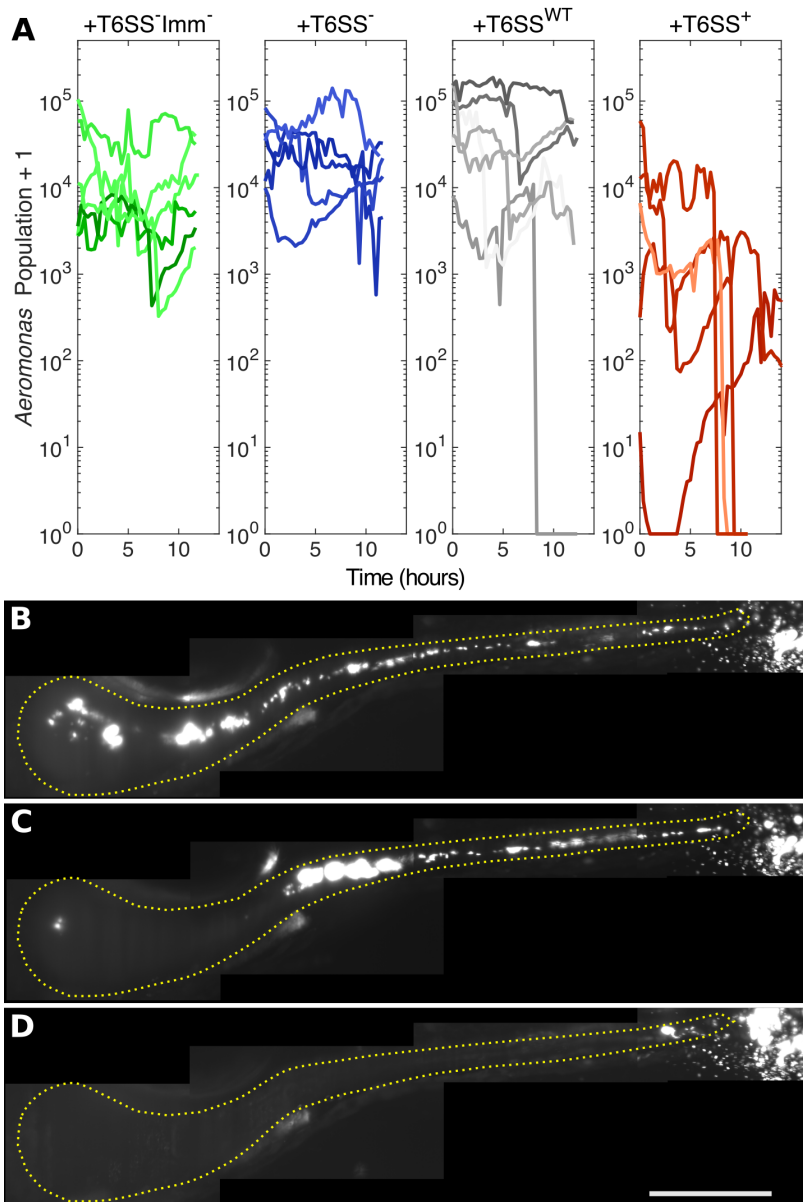


**Figure 3.3** (A) Time-series of *Aeromonas* populations in larval zebrafish intestines when challenged by different strains of *Vibrio cholerae*, derived from light sheet fluorescence imaging. Beginning 8 hours after *Vibrio* inoculation, fish were imaged every 20 minutes for 12-17 hours. Each curve is from a different zebrafish. When invaded by T6SS<sup>+</sup> *V. cholerae*, overall *Aeromonas* abundance is low, and collapses in population of over an order of magnitude are evident. (B,C,D) Maximum intensity

projections of a 3D light sheet image stack of *Aeromonas* in a larval zebrafish intestine invaded by T6SS<sup>+</sup> *V. cholerae* at 9.3, 10.7, and 16.3 hours after the start of imaging. A collapse of the *Aeromonas* population is evident as time progresses. Yellow dotted lines roughly indicate luminary boundary. Scale bar: 200  $\mu\text{m}$ .

### **3.5 Constitutively expressed T6SS alters the intestinal movements of larval zebrafish in an ACD-dependent manner**

The larval zebrafish intestine, like those of other animals, has periodic propagative contractions that drive the motion of dense aggregates of *Aeromonas* and can ultimately cause their ejection (Wiles et al., 2016). We tested whether the collapses in the *Aeromonas* populations observed in the T6SS<sup>+</sup> competition (Fig. 3B-D) could be due to greater gut motility. We compared intestinal movements of germ-free fish and fish mono-associated with the various *V. cholerae* strains using differential interference contrast microscopy (DICM), which allowed direct visualization of the intestinal epithelial tissue and lumenal space (Fig. 4A) (Baker et al., 2015). Then, we used image velocimetry techniques to quantify the the frequency and amplitude of intestinal contractile waves (Wiles et al., 2016; Zac Stephens et al., 2016). None of the strains altered the frequency of peristaltic contractions, compared to germ-free fish (Fig. 4B). The amplitude of the contractions, however, was greatly enhanced in the fish colonized with T6SS<sup>+</sup> strain, but not other strains (Fig. 4C, Supplemental Movies 7-8). The magnitude of the effect, roughly a 200% increase in the amplitude of contractions compared to germ-free fish, was remarkable and unexpected. For comparison, treatment



with the neurotransmitter acetylcholine or deletion of all enteric neurons induces at most a change of roughly 40% in peristaltic amplitude (Zac Stephens et al., 2016).

Though this T6SS-dependent alteration of host gut motility was unexpected, there are well-established precedents for T6SS-mediated *V. cholerae* interactions with eukaryotic cells driven by an actin crosslinking domain (ACD) present in the C-terminus of the VgrG-1 spike protein of the T6 secretion apparatus (Zhao et al., 2018). We hypothesized that the ACD might also be responsible for the larger amplitude of gut motility. To test this hypothesis, we deleted the ACD of *vgrG-1* in the constitutive T6SS-expressing *V. cholerae* T6SS<sup>+</sup> strain (see Methods). When we mono-colonized zebrafish larvae with T6SS<sup>+</sup> ACD<sup>-</sup> *V. cholerae*, we observed no increase in either the frequency or amplitude of intestinal contractions compared to germ-free fish (Fig. 4B,C). This strain, however, maintained the ability to kill *Aeromonas in vitro* at a rate similar to that of T6SS<sup>+</sup> strain, which indicates an otherwise functional T6SS (Fig 4D). Therefore, the VgrG-1 ACD is specifically necessary for the increase of amplitude in intestinal contractions observed in fish mono-colonized with the T6SS<sup>+</sup> strain.

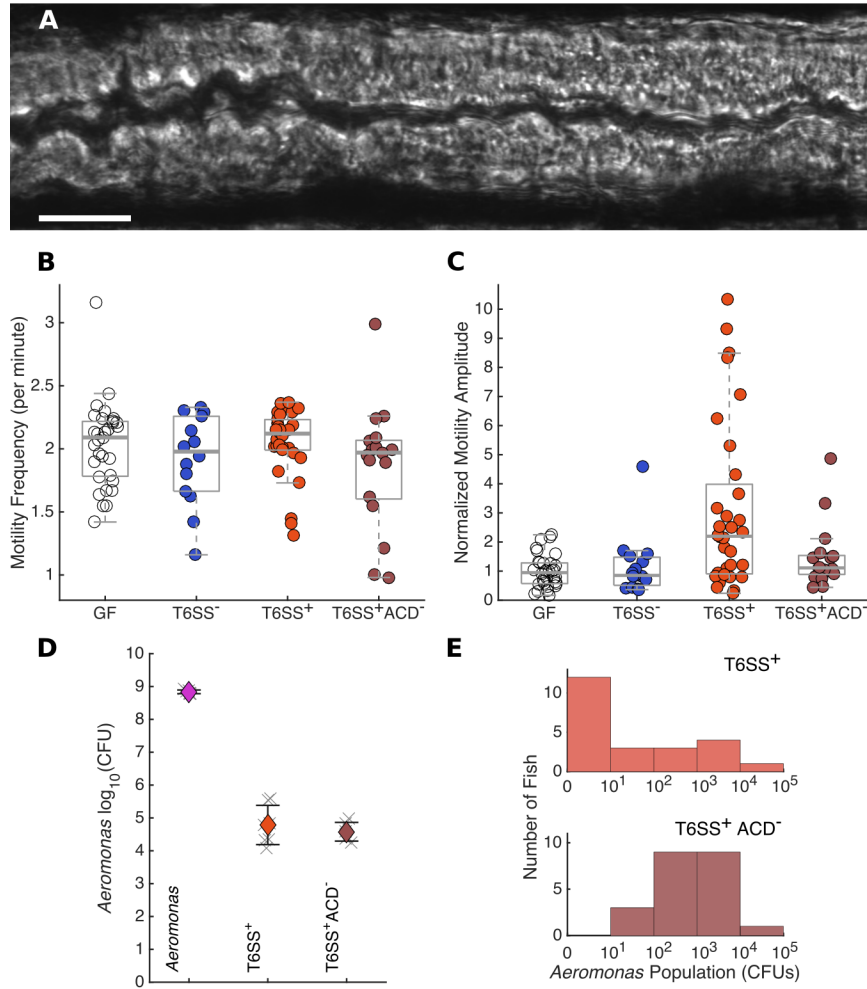


**Figure 3.4** (A) A DIC image of a portion of a larval zebrafish intestine. Scale bar: 50  $\mu\text{m}$ . (B) Frequency of periodic gut motility for germ-free fish and fish mono-associated with T6SS<sup>-</sup>, T6SS<sup>+</sup>, and T6SS<sup>+</sup>ACD<sup>-</sup> strains. (C) Gut motility amplitudes under the same conditions as panel (B), normalized by the mean value in germ-free fish. Fish associated with T6SS<sup>+</sup> show far greater gut motility amplitude than T6SS<sup>-</sup>, T6SS<sup>-</sup>ACD<sup>-</sup>, or germ-free fish. (D) *In vitro* killing rates of *Aeromonas* by T6SS<sup>+</sup> and T6SS<sup>+</sup>ACD<sup>-</sup> *Vibrio cholerae* strains. (E) Histogram of *Aeromonas*

abundances in the zebrafish gut 24 hours after potential invasion by T6SS<sup>+</sup> (the same data as in Figure 2C) and T6SS<sup>+</sup>ACD<sup>-</sup> strains. The peak abundances are roughly 0 when followed by the T6SS<sup>+</sup> strain, but 10<sup>2</sup>-10<sup>3</sup> CFU/gut when followed by the T6SS<sup>+</sup>ACD<sup>-</sup> strain.

We then tested the ability of T6SS<sup>+</sup> ACD<sup>-</sup> *V. cholerae* to invade an intestinal *Aeromonas* population using the same zebrafish invasion assay described above. While the *Aeromonas* population drops precipitously following T6SS<sup>+</sup> *V. cholerae* introduction, *Aeromonas* after T6SS<sup>+</sup> ACD<sup>-</sup> *V. cholerae* introduction remained abundant, averaging approximately 1000 CFU per fish ( $N = 31$  fish) similar to the numbers seen when challenged by T6SS<sup>-</sup> strains (Fig. 4E, F). T6SS<sup>+</sup> ACD<sup>-</sup> *V. cholerae* was nonetheless present in the gut at high abundance, approximately 10<sup>4</sup> CFU/gut, supporting that deleting the ACD specifically compromises the ability to induce the host intestinal movements and expel the commensal. This experiment demonstrated that removing the T6SS actin crosslinking domain eliminates *V. cholerae*'s ability to displace a competitor, despite an otherwise functional T6SS capable of killing *in vitro*. Taken together, these results show that the ability of *V. cholerae* to dominate a gut colonized by *Aeromonas* works specifically by increasing the amplitude of host peristalsis in a manner dependent on the VgrG-1 ACD.

### **3.7 Materials and Methods**

#### **Ethics statement**

All experiments involving zebrafish were carried out in accordance with protocols approved by the University of Oregon Institutional Animal Care and Use Committee and followed standard methods.

#### **Gnotobiotic techniques**

Wild-type larval zebrafish were derived devoid of microbes as previously described in (Milligan-Myhre et al., 2011). In brief, fertile eggs were collected and placed in a sterile antibiotic embryo media solution consisting of 100 µg/ml ampicillin, 250 ng/ml amphotericin B, 10 µg/ml gentamycin, 1 µg/ml tetracycline, and 1 µg/ml chloramphenicol for approximately six hours. The eggs were then washed in a sodium hypochlorite solution and a polyvinylpyrrolidone–iodine solution. Washed embryos were distributed in sets of 15 into tissue culture flasks containing 15µl of sterile embryo media. Flasks of larval zebrafish were inspected for sterility prior to their use in experiments.

#### **Bacterial strains and culture conditions**

*Aeromonas veronii* (ZOR0001, PRJNA205571) and *Vibrio* (ZWU0020, PRJNA205585) were isolated from the zebrafish intestinal tract as previously described (Zac Stephens et al., 2016). These strains were fluorescently labeled with EGFP or dTomato for imaging experiments with methods similar to those described previously (Wiles et al., 2016).

All *V. cholerae* strains were derivatives of El Tor C6706 str-2. Bacterial cultures were routinely grown at 30°C or 37°C in lysogeny broth (LB) with shaking, or statically on LB agar. In-frame deletion mutants and promoter-replacements in *V. cholerae* were constructed using the allelic exchange method described previously (Choi et al., 2005). Standard molecular biology-based methods were utilized for DNA manipulations. DNA modifying enzymes and restriction nucleases (Promega and New England Biolabs), Gibson assembly mix (New England Biolabs), Q5, Phusion and OneTaq DNA Polymerases (New England Biolabs) were used following the manufacturer's instructions. All recombinant DNA constructs were verified by Sanger sequencing (Eurofins).

### **Culture-based quantification of bacterial populations**

Germ-free larval zebrafish were inoculated with select bacterial strains as in previous work (Rolig et al., 2015; Wiles et al., 2016). Bacteria were grown on a shaker in Luria Broth for 10-14 hours at 30 °C. Bacteria were prepared for inoculation by pelleting for two minutes at 7000g and were washed once in sterile embryo media prior to inoculation. An inoculum of 10<sup>6</sup> CFU/ml was used for *Aeromonas* (ZOR0001, PRJNA205571) and *Vibrio* (ZWU0020, PRJNA205585) strains and 10<sup>7</sup> CFU/ml for *Vibrio cholerae* strains. Bacterial inoculums were added directly to tissue culture flasks containing germ-free larval zebrafish.

### **In vitro measurements of bacterial competition**

For *in vitro* killing assays, bacterial strains were inoculated from glycerol stock and shaken in lysogeny broth (LB) at 30 °C or 37 °C overnight. The cells were then harvested, washed in sterile phosphate buffered saline (PBS) twice and normalized to OD<sub>600</sub>=1 in PBS. Pairs of strains were mixed 1:1, and 25 µl of the liquid was spotted onto a 0.20 µm diameter porous nylon membrane filter (Millipore) placed on an LB agar plate. After allowing them to dry, plates were incubated at 37 °C for 3h. Each membrane was then carefully removed from the agar plate and vortexed in sterile PBS for 1 min. The killing rate was assessed by comparing the target cell numbers before and after incubation by plating and counting colony forming units (CFUs). An antibiotic resistant marker (streptomycin or gentamicin) inserted into the target strain chromosome enabled discrimination of target cells for CFU counting.

For *in vitro* time lapse fluorescence microscopy, bacterial strains were inoculated from glycerol stocks and shaken in LB at 30 °C or 37 °C overnight. The overnight culture was brought back to exponential phase by diluting 70 µl culture into 4 ml fresh LB and shaking for 3h at 30 °C. Frames and coverslips (Thermo scientific) were used to form an agar pad using 1% low-melting point agarose in PBS. Exponential phase cells were centrifuged at 6000 rpm for 1 min and resuspend in fresh LB. One microliter of mixed cells (v:v ratio = 1:1) was spotted onto the agar pad, allowed to dry, and then covered with a coverslip. The fluorescent labeled cells were imaged in each of two fluorescence channels (mTFP and mKO) every ten minutes using a 63x oil immersion objective lens

on an inverted wide-field fluorescent microscope (Zeiss AxioObserver.Z1). Acquired images were processed with customized Matlab scripts.

### **Light sheet fluorescence microscopy**

Light sheet microscopy was performed on a home-built light sheet microscope based on the design of Keller et al. (Keller et al., 2008) and described in (Jemielita et al., 2014; Taormina et al., 2012). In brief, the beams from either of two continuous-wave lasers (Coherent Sapphire, 448 nm and 561 nm) are rapidly scanned using a galvanometer mirror and demagnified to create a thin sheet of excitation light perpendicular to and at the focus of an imaging objective lens. The specimen is moved through this sheet in one-micron steps and fluorescence emission is captured to create a three-dimensional image. To image the entire larval zebrafish gut, four sub-regions are imaged and later manually registered and stitched. All exposure times were 30 ms and excitation laser power was set to 5mW measured at the laser output. A 5.5 Mpx sCMOS camera (Cooke Corporation) was used for all light sheet imaging, and a 40x 1.0NA objective lens (Zeiss). For time series imaging, scans occurred at 20-minute intervals for 12-17 hour durations.

### **Sample handling and mounting for imaging**

Specimens were prepared for imaging as previously described in (Jemielita et al., 2014). Larval zebrafish were anesthetized using tricaine methanesulfonate at 120µg/ml, placed in melted 0.5% agarose gel at no more than 42 °C, and pulled individually into glass capillaries. Each capillary was then mounted on a holder on a computer-controlled translation stage, and each fish was extruded in a plug of gel into a specimen chamber

filled with sterile embryo medium and tricaine methanesulfonate. The fluid in the specimen chamber was maintained at 28 °C. All time series experiments were performed overnight beginning in the evening.

### **Imaging-based quantification of bacterial populations**

*In vivo* gut bacterial populations were quantified from light sheet images using an analysis pipeline described in (Jemielita et al., 2014). In brief, bacterial aggregates and individual bacteria were separately identified. The number of bacteria per aggregate is estimated by dividing the total fluorescence intensity of the clump by the average intensity of individuals. Discrete individuals were detected using a wavelet-based spot detection algorithm, with autofluorescent host cells and other non-bacterial identified objects rejected using a support vector machine based classifier augmented with manual curation.

### **Identification of population collapse events**

Collapses of bacterial populations were identified from light sheet microscopy time series images and visually confirmed as described in (Wiles et al., 2016). Population collapses in *Aeromonas* were defined as a decrease in the total population of at least a factor of 10 in one time step (20 minutes), together with at least a factor of 2 decrease relative to the original population at the next time step, the latter to false positives from single bad datapoints.



### **Intestinal motility measurements**

Intestinal motility in larval zebrafish was imaged using Differential Interference Contrast Microscopy (DICM) as described in (Baker et al., 2015). Videos were recorded at 5 fps. A velocity vector field was determined from the image series using image velocimetry, and the amplitudes and frequencies of gut motions along the anterior-posterior (AP) axis were obtained using the analysis pipeline described in (Ganz et al., 2018). In brief: The AP component of the vector field was averaged along the dorsal-ventral direction, resulting in a scalar motility measure at each position along the gut axis and at each time point. The frequency of gut contractions was calculated as the location of the first peak in the temporal autocorrelation of the motility. The amplitude was calculated as the square root of the spatially averaged power spectrum at the previously determined frequency, providing the magnitude of the periodic motion.

### **3.6 Discussion**

We have shown that *V. cholerae* can employ its type VI secretion system to amplify the intestinal contractions in a zebrafish host and induce the expulsion of a resident microbiota of the commensal genus *Aeromonas*. The coupling of T6SS activity to host contractions depended on an actin crosslinking domain (ACD) of the T6SS apparatus; when the ACD was deleted, *V. cholerae* could no longer induce enhanced host contractions and dense *Aeromonas* communities remained in the gut. Deleting the ACD did not affect the ability of *V. cholerae* to kill *Aeromonas* on contact; nor did it impact the ability of *V. cholerae* to enter and occupy the intestinal host, at least initially. *V. cholerae* itself seems unaffected by the enhanced intestinal motility, which could be due to its ability to remain planktonic and motile inside the zebrafish gut (Fig. 1C, Supp. Movie 1),

which mirrors that of the commensal *Vibrio* ZWU0020 (Wiles et al., 2016, 2017). Taken together, our results show that an enteric colonizer (*V. cholerae*) can use a previously undiscovered host-microbe interaction (T6SS-dependent enhancement of gut contractions) to influence the population dynamics of a competitor (*Aeromonas*).

This newly revealed physiological function of the T6SS adds to the already rich variety of mechanisms known to orchestrate the ecology of the microbiome (Foster et al., 2017), and highlights the role of host intestinal peristalsis in shaping gut population dynamics, an emergent theme in contemporary microbiome research (Cremer et al., 2016, 2017; Wiles et al., 2016, 2017). The T6SS in itself has received deserved attention for its dramatic role in contact-mediated inter-bacterial toxicity (Verster et al., 2017) and potential implications in mediating interbacterial competition within the animal microbiome (Coyne et al., 2014; Russell et al., 2014a; Wexler et al., 2016; Zhao et al., 2018). Our findings suggest the additional possibility that gut colonizing bacteria can use T6SS to manipulate the host. Given the prevalence of T6SS among bacteria, such host manipulations could be a common tactic to indirectly influence interbacterial competition. Moreover, exogenous delivery of T6SS proteins, or their engineering into otherwise beneficial microbes, could offer a new path to therapeutic modulation of human gastrointestinal activity.

Our observations may also inform our understanding of T6SS regulation. For many patient-derived “wild type” *V. cholerae* isolates, robust T6SS activity can be triggered by chitinous material (Bernardy et al., 2016; Borgeaud et al., 2015; Watve et al., 2015) that constitutes crab shells, zooplankton exoskeletons, and marine snow commonly colonized by *Vibrios* in aquatic environments (Bartlett and Azam, 2005; Pruzzo et al.,

2008). We found that wild type C6706 *V. cholerae*, but not T6SS<sup>-</sup> derivatives was capable of modest killing of *Aeromonas in vitro* (Fig. 2A), consistent with results observed prior for C6706 T6 killing of an *E. coli* target (Bernardy et al., 2016). We also observed small reductions in *Aeromonas* counts and rare extinction events *in vivo* (Fig 2C and Fig. 3A). Since the germ-free zebrafish used here were not provided with a chitin source, it is interesting to speculate that endogenous chitin production recently documented within the juvenile zebrafish gut (Tang et al., 2015) is inducing the wild type *V. cholerae* T6-mediated activity observed here. Further studies will determine the contribution that chitin signaling plays in T6 expression by *V. cholerae* in fish intestinal environments.

Most directly, our work sheds a new light on the role of the T6SS in the colonization by *V. cholerae* of a vertebrate host. The ability of the T6SS to amplify host intestinal mechanics was previously undetected, likely for three reasons. First, the development of cholera in humans is a complex, multifactorial process in which the role of T6SS may be confounded by other factors, most importantly the strong effects of the cholera toxin. Second, the animal models typically used in cholera research are not native cholera hosts, and the mechanisms of their colonization may be different. Fish, however, naturally host *V. cholerae*, and because zebrafish colonization depends less on other factors we could detect the effects of T6SS on intestinal movements, and we could then use genetically modified *V. cholerae* strains to confirm the molecular mechanism. Third, the zebrafish model allows direct, quantitative, *in vivo* imaging using modern microscopy methods, in contrast to indirect, static, DNA- or RNA-sequencing-based assays typically used to study mouse or human microbiomes. *In vivo* imaging greatly facilitates

observations of intestinal activity and enabled the discovery of sudden spatiotemporal changes in bacterial distributions. How our findings may map onto *V. cholerae* colonization in humans is unknown, but a role for T6SS-mediated activity is certainly plausible. Establishing this will take further investigation, as will the design of therapeutics that target the T6SS to prevent colonization in humans or in environmental reservoirs such as fish. Nonetheless, our results enhance our understanding of the strategies and abilities of *V. cholerae*, a pathogen that continues to impact millions of people worldwide.

The discoveries discussed in this chapter would not have been possible without advanced microscopy techniques and many labor-intensive hours spent preparing samples and mounting them for imaging. In order to make processes like this more efficient and less laborious, we have developed a new high-throughput microscope to allow rapid, automated light sheet fluorescence imaging of large numbers of samples. This microscope, as well as examples of its data collection capabilities, are the subject of the next chapter.

## CHAPTER IV

### AUTOMATED HIGH-THROUGHPUT LIGHT SHEET MICROSCOPY

This chapter contains unpublished co-authored material; it has been adapted from S. L. Logan, C. Dudley, R. P. Baker, E. A. Hay, M. J. Taormina and R. Parthasarathy, “Automated High-Throughput Light-Sheet Microscopy of Larval Zebrafish” Preprint: *bioRxiv*, 392316 (2018). In this work, I contributed to designing the research, performing the research, analyzing the data, and writing the paper.

#### 4.1 Introduction

Light sheet fluorescence microscopy (LSFM) is a powerful tool for examining the three-dimensional structural and temporal dynamics of living systems. In LSFM, a thin sheet of laser light excites fluorophores in a sample. Scanning the sample through the sheet enables fast, three-dimensional imaging with low phototoxicity, high resolution, and a wide field of view (Huisken, 2012; Keller et al., 2008, 2014; Power and Huisken, 2017; Santi, 2011). Imaging with LSFM has enabled numerous studies of embryonic development (Tomer et al., 2012; Weber et al., 2017), neural activity (Keller and Ahrens, 2015), microbial dynamics (Logan et al., 2018; Parthasarathy, 2018; Wiles et al., 2016), and other phenomena. A large body of work has focused on improving the optical capabilities of light sheet imaging, for example using structured illumination (Chang et al., 2017; Chen et al., 2014), multiple lens pairs (Tomer et al., 2012), two-photon excitation (Truong et al., 2011), and other techniques. However, current light sheet

fluorescence microscopes have significant constraints related to throughput and sample handling that, we argue, have placed much greater limitations on their scientific utility than issues of spatial or temporal resolution. The majority of existing light sheet fluorescence microscopes, both commercial and non-commercial, are designed to hold a single specimen. A few instruments (including one from the authors of this paper) can hold up to six specimens for sequential imaging. Moreover, light sheet fluorescence microscopy typically requires extensive sample preparation and manual sample mounting, most commonly by embedding specimens in agarose gels. Examination of large numbers of specimens is therefore slow and difficult, which is especially important given the high level of inter-individual variability found in many complex biological processes. Increasing the pace of insights into developmental biology, multicellular biophysics, or microbial community structure will require faster and simpler acquisition of three-dimensional imaging datasets. To date, there exists only one report of an automated light sheet microscope that makes use of fluidic positioning of live animals (Gualda et al., 2015); its throughput (specimens per hour) is not stated, and though its ability to image larval zebrafish is clear, the total number of animals examined was only twelve. In contrast, automated, high-throughput methods have been integrated with other types of microscopes, including confocal microscopes (Hwang and Lu, 2013; Pardo-Martin et al., 2010; Yanik et al., 2011), about which we comment further in the Discussion. Our system adopts and builds upon these, especially the confocal-based setup of (Pardo-Martin et al., 2010).

To address the issues described above, we developed a light sheet fluorescence microscope capable of automated, high-throughput imaging of live specimens. Our

instrument uses fluidic control and image-based registration to rapidly but precisely position specimens for light sheet scans and subsequently remove them from the imaging area. We characterize the optical quality of our instrument, and demonstrate its capabilities by rapidly imaging immune cells in dozens of larval zebrafish. While the spatial resolution of our microscope does not equal that of current “low-throughput” light sheet microscopes, it is more than sufficient for determining cellular distributions. Moreover, we argue that the tradeoff of lower resolution for higher throughput is worthwhile given the large variance in most biological datasets.

We illustrate the utility of the instrument by imaging neutrophils in dozens of larval zebrafish. Neutrophils are an important and highly dynamic cell type of the innate immune system. These cells migrate to sites of damage or infection and recognize and kill pathogenic microbes (Mayadas et al., 2014). Zebrafish are a well recognized model organism for studying neutrophil responses (Galindo-Villegas, 2016; Meijer and Spaik, 2011), and prior work has uncovered changes in neutrophil distributions in response to wound-induced chemotaxis (Kadirkamanathan et al., 2012), drugs that lead to symptoms similar to human enterocolitis (Oehlers et al., 2011), and stimulation by gut microbes or bacterial lipopolysaccharide (LPS) (Bates et al., 2007; Rolig et al., 2015), to list a few of many examples. Quantifying even basic properties such as neutrophil abundances over large extents for the dozens of specimens required given the high variance between individuals often necessitates slow confocal imaging or painstaking histological sectioning or gut dissection (Bates et al., 2007; Kanther et al., 2014; Rolig et al., 2015). These sorts of studies will be greatly facilitated by instruments that can provide large-scale 3D imaging of automatically detected and imaged specimens.

We show, as expected, a high degree of variation between fish in total neutrophil number and an increase in its mean value following LPS exposure, as well as spatial clustering of neutrophils in two distinct regions near the swim bladder. While our instrument is optimized for imaging of larval zebrafish, the design could easily be modified for rapid imaging of a wide range of biological and non-biological samples, which should broaden the impact of light sheet microscopy in a variety of fields.

## **4.2 Instrument design, development, use, and limitations**

### **Instrument design**

The light sheet portion of the microscope closely follows the design of Keller et al (Keller et al., 2008); a rapidly-scanned galvanometer creates a sheet of light for fluorescence excitation, and emitted light is captured by a camera perpendicular to the plane of the sheet (Fig. 1A). In conventional light sheet fluorescence microscopes, gel-mounted specimens are introduced vertically in between horizontal lenses. To achieve high throughput, we use a continuous fluidic path through plastic tubing and glass capillaries for transport as well as imaging, detailed below. If the fluidic path were oriented vertically, specimens would gravitationally drift during imaging. Therefore, we adopted a geometry in which specimens are transported horizontally and the sheet plane is vertical (Fig. 1A,B). To allow this arrangement, we designed an elongated sample chamber with windows oriented below and perpendicular to the sample (Fig. 1B,C). Before entering the imaging chamber, specimens flow through a system of 0.7 mm diameter plastic tubing at a typical flow rate of 1 ml/min, or 4 cm/sec (Fig. 1). Flow



speed and direction are controlled by a syringe pump (Fig. 1); see Supplemental Methods for a parts list and descriptions.

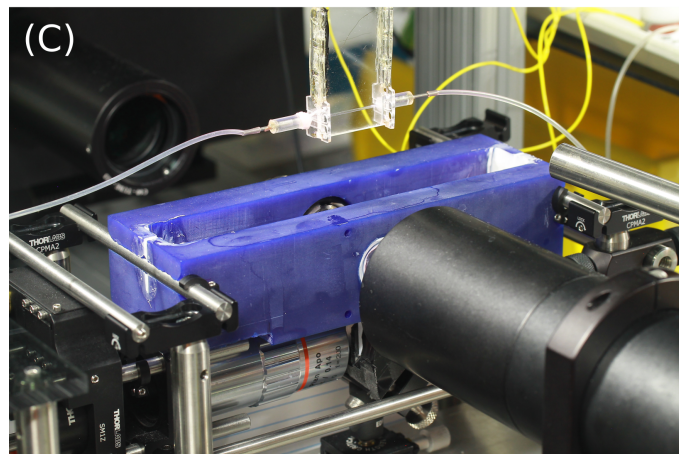
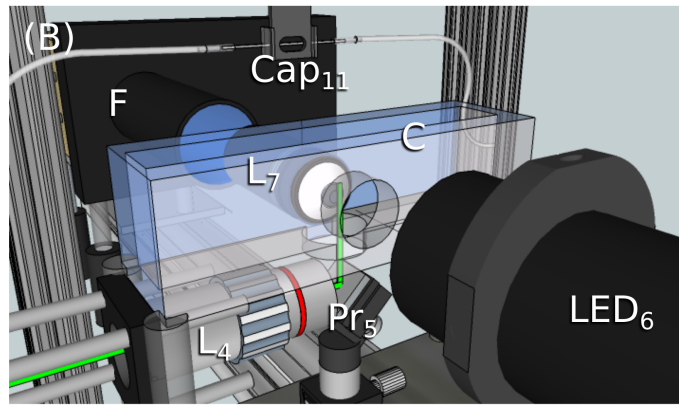
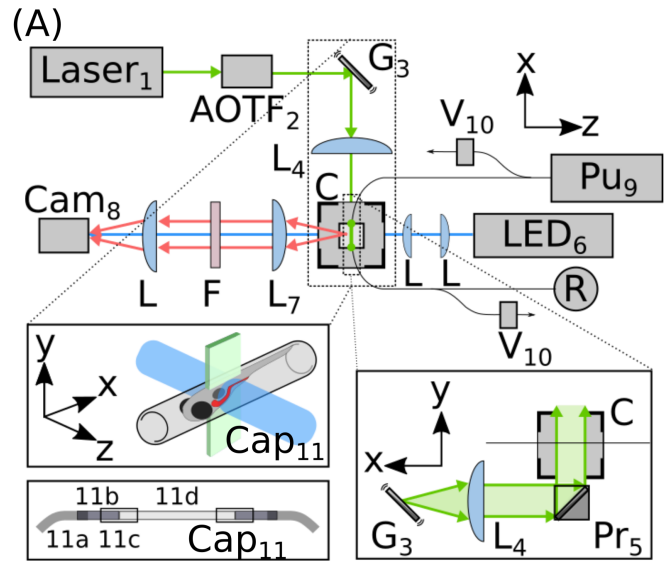


**Figure 4.1. Instrument design.** (A) Schematic of the instrument design, with labels corresponding to the parts list in Table 1. The excitation laser line is selected by an acousto-optic tunable filter (AOTF<sub>2</sub>), then directed to a galvanometer mirror (G<sub>3</sub>) and objective lens (L<sub>4</sub>) to create a time-averaged sheet of light in the sample chamber (C) via a prism (Pr<sub>5</sub>). Specimens flow through a system of tubing controlled by a syringe pump (Pu<sub>9</sub>) and valves (V<sub>10</sub>) and are automatically positioned in a square-walled capillary (Cap<sub>11</sub>) for imaging. Bright field images are used for positioning the sample and are illuminated with an LED (LED<sub>6</sub>). After imaging, specimens are directed into a reservoir (R). (B) Schematic of the imaging area. The 3D-printed sample chamber (C), prism (Pr<sub>5</sub>), and imaging capillary (Cap<sub>11</sub>) are apparent. (C) Photograph of the imaging area corresponding to the schematic in (B).

Inside the imaging chamber, specimens flow into a square-walled glass capillary in front of the imaging objective where they are automatically detected by bright field microscopy. Specimens are rapidly stopped using computer-controlled valves on either side of the imaging chamber, with a precision of approximately 1 mm in position, comparable to the length of a larval zebrafish. Fine positioning is performed by iterated movement of the capillary by a computer-controlled stage, brightfield imaging, and comparison of images with a previously assembled image library (see Methods) (Fig. 2 A,B). The travel range of the capillary on the stage allows movement of up to 30 mm in the x-direction. Like many studies, ours make use of larval zebrafish as a model

organism; strong features such as eyes and the swim bladder enable straightforward correlation-based registration, with a precision of about 20  $\mu\text{m}$  as described below. This approach should be applicable to any specimen with a roughly stereotypical anatomy. The specimen is not rotated about the tube axis; we comment further on this in the Discussion section.

Once positioned, specimens are automatically imaged using LSM. The imaging chamber has sufficient depth, 35 mm, that the capillary can be scanned through the sheet by a motorized stage. In our setup, repeated scans with up to three excitation wavelengths are possible; this is limited simply by the number of available laser lines. The precision of the automated positioning enables scans to be taken of particular regions, for example the larval gut, as shown below. After imaging, specimens flow into a collection reservoir and subsequent specimens are automatically positioned for imaging. We provide a movie of the instrument in operation as Supplementary Video S1. A complete parts list is provided as Table 1, in Supplemental Methods.

### **Optical quality**

Our instrument uses glass capillaries for specimen mounting, rather than more conventional gel embedding. The square cross-section of these capillaries should lead to less distortion than more common cylindrical capillaries. To assess the optical quality of our setup, we measured the point spread function (PSF) by imaging 28 nm diameter fluorescent microspheres dispersed in oil in these capillaries (see Methods for details). The diffraction-limited width of the particles in the sheet plane ( $xy$ ), assessed as the

standard deviation of a Gaussian function fit to the particle's intensity profile, is  $0.6 \mu\text{m}$ , and the width along the detection axis ( $z$ ) is  $3.4 \pm 0.6 \mu\text{m}$ , consistent with the expected sheet thickness of our setup (Fig. 2 C,D).

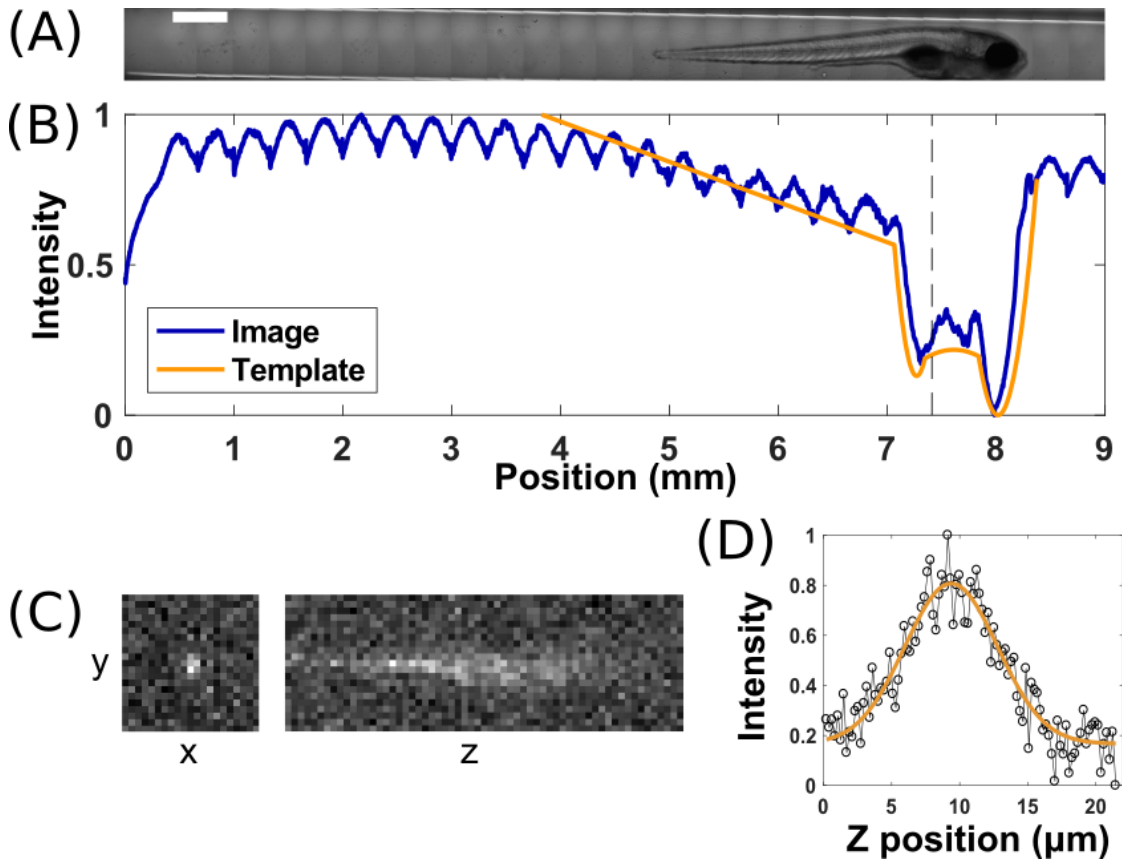


**Figure 4.2. Specimen positioning and image quality.** (A) Composite brightfield image of a larval zebrafish positioned in a glass capillary. Scale bar:  $50 \mu\text{m}$ . (B) Normalized intensity averaged along the short axis of the brightfield image, and the intensity of the template image that best matches the fish in (A). Cross-correlation with the template is used to automatically position the fish for light sheet fluorescence imaging. (C)

Light sheet fluorescence images of a 28 nm diameter fluorescent microsphere, showing  $x$ - $y$  and  $z$ - $y$  planes centered on the particle. (D) Line-scan of intensity along the detection axis ( $z$ ) through a fluorescent microsphere, with a Gaussian fit showing a width of approximately 3  $\mu\text{m}$ .

### **Data collection capabilities**

Using this system, we can image approximately 30 larval zebrafish per hour, obtaining from each a 666 x 431 x 1060  $\mu\text{m}$  ( $x$ ,  $y$ ,  $z$ ) three-dimensional scan, a marked improvement over manual mounting and imaging that, even by a skilled researcher, is limited to about 5 fish per hour. The triggering accuracy is about 90%, with roughly 10% of detected objects being bubbles or debris that are easily identified after imaging. On average, 81% of larval fish are automatically positioned correctly in front of the imaging objective. The remaining 19% correspond to multiple fish being in the field of view, or other positioning errors. Importantly, the majority of the run time of the instrument is spent obtaining light sheet fluorescence images, and is not dominated by specimen positioning. In the batch of  $N=41$  fish whose neutrophil distributions were imaged in experiments described below, for example, the flow, detection, and positioning of the specimens occupied only approximately 30 seconds per fish. In the limit of zero imaging time (e.g. for very bright signals or small regions of interest), the system could therefore record data from up to about 120 specimens per hour in the absence of triggering or positioning errors, or about 90 specimens per hour with the present system performance.

### **Neutrophils in larval zebrafish**

To demonstrate the capabilities of the instrument, we imaged fluorescent neutrophils in larval zebrafish at 5 days post-fertilization (dpf), focusing especially on the number of these immune cells and their distribution near the anterior of the intestine. Specifically, these were fish engineered to express green fluorescent protein (GFP) under the promoter myeloperoxidase, an enzyme primarily produced in neutrophils (Renshaw et al., 2006).

### **Positioning accuracy**

To assess the positioning accuracy of our instrument, we performed automated scans of larval zebrafish with GFP-expressing neutrophils, and then reloaded the same fish and re-scanned them. Changes in the neutrophil positions are due to both imaging error and to motion of the neutrophils during the intermediate time. (Neutrophils are highly motile cells, crawling through tissue and also entering or leaving tissue via the bloodstream.) For five twice-scanned fish, we manually identified three neutrophils that were unambiguously the same in each scan (i.e. not newly entered or departed). For these neutrophils, the within-fish standard deviations of the changes in position provide a measure of the biological variation, e.g. from neutrophil motion. These were  $5.3 \pm 3.5 \mu\text{m}$ ,  $11.6 \pm 9.0 \mu\text{m}$ , and  $40.0 \pm 36.4 \mu\text{m}$ , for  $x$ ,  $y$ , and  $z$ , respectively, where  $x$  is the flow direction and  $z$  is perpendicular to the light sheet. The standard deviation between fish of the mean neutrophil positions provides a measure of the instrumental variation, e.g. from imperfect positioning. These were  $18.9 \pm 6.7 \mu\text{m}$ ,  $56.1 \pm 19.9 \mu\text{m}$ , and  $52.6 \pm 18.6 \mu\text{m}$  for  $x$ ,  $y$ , and  $z$ , respectively. Along the capillary axis, therefore, the fish positioning is reproducible to within about  $20 \mu\text{m}$ . The larger variance in  $y$  and  $z$  is expected, as we are

not explicitly detecting location along these axes, and because there can be specimen rotation about the  $x$ -axis. Overall, therefore, global positioning uncertainty is on the order of a cell diameter for cells such as neutrophils.

### **Neutrophil number and variance**

In total, we imaged 41 fish, obtaining from each a single  $666 \times 431 \times 1060 \mu\text{m}$  three-dimensional image in which neutrophils were readily evident (Fig. 3A). Brightfield images are captured and saved prior to fluorescence imaging; a set of four such images, demonstrating their appearance and variance, are provided as Supplemental Figure 1. The strong GFP signal enabled automated identification of neutrophils by standard segmentation methods. Corroborating previous work done by manual dissection of zebrafish (Rolig et al., 2015), we found a high degree of variation in neutrophil number between specimens, with the standard deviation being 30% of the mean (Fig. 3B). Furthermore, we found that neutrophils tend to cluster in two distinct regions: adjacent to the swim bladder on both the anterior and posterior (Fig. 3C). Notably, the total GFP intensity in a fish is weakly correlated with the number of neutrophils, with a coefficient of determination  $R^2 = 0.4$ , indicating that a simple measure of overall brightness, as could be assessed without three-dimensional microscopy, would provide a poor diagnostic of the actual abundance of immune cells (Fig. 3D). We also compared neutrophil counts determined from two-dimensional maximum intensity projections of the full three-dimensional image stacks, mimicking images that would be obtained from simple widefield fluorescence microscopy. This yielded a number of neutrophils that was on average  $0.76 \pm 0.02$  of that from the three-dimensional counts, indicating as expected that

some neutrophils are behind others in the three-dimensional space of the specimen, and hence require three-dimensional imaging for accurate assessment.

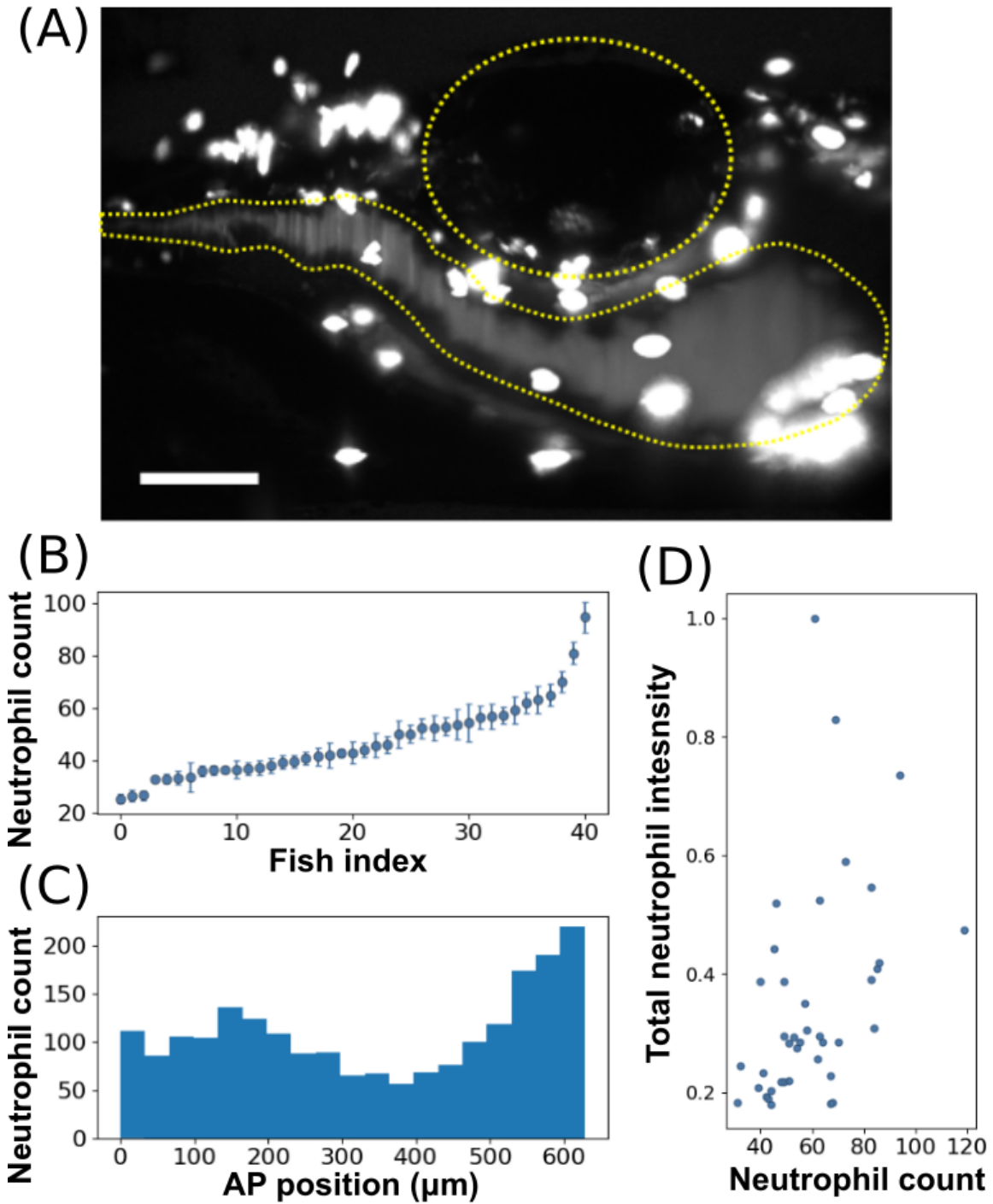




**Figure 4.3. Imaging neutrophils in larval zebrafish.** (A) A maximum intensity projection of a three-dimensional light sheet fluorescence image of GFP-expressing neutrophils near the intestine of a 5 dpf larval zebrafish. The 3D scan is provided as Supplemental Movie 2. The intestine and swim bladder are roughly outlined by the yellow dotted lines. Scale bar: 100  $\mu\text{m}$ . (B) The total number of neutrophils in each fish; the x-axis is ordered by neutrophil count. (C) Neutrophil count along the anterior-posterior dimension, summed over all fish examined ( $N=41$ ). The x-axis corresponds approximately to the horizontal range of (A). (D) The total intensity of the detected neutrophils per fish vs the total number of neutrophils in that fish. The two measures are weakly correlated with a coefficient of determination  $R^2 = 0.4$ .

In addition, we examined neutrophil number in response to exposure of larval zebrafish to soluble lipopolysaccharide (LPS), the major component of the outer membrane of gram negative bacteria, known from earlier studies to stimulate an inflammatory immune reaction (Bates et al., 2006, 2007). As above, we detected and scanned transgenic zebrafish with GFP-expressing neutrophils, exposed to LPS in their flask water at a concentration of 150  $\mu\text{g}/\text{ml}$  for 0 (control), 2, and 24 hours prior to imaging. As above, neutrophil number shows a large degree of variability. At 5 dpf, we detected  $85.0 \pm 17.0$  ( $N = 13$ ) and  $87.6 \pm 27.6$  ( $N = 14$ ) (mean  $\pm$  standard deviation) neutrophils in fish subjected to no LPS and LPS for 2 hours, respectively; indicating no discernible change. At 6 dpf, we detected  $95.1 \pm 23.4$  ( $N = 21$ ) and  $114.2 \pm 38.1$  ( $N = 19$ )

in the control and 24-hour LPS-treated fish, respectively, indicating an increase in the mean neutrophil count by a factor of  $1.2 \pm 0.1$ .

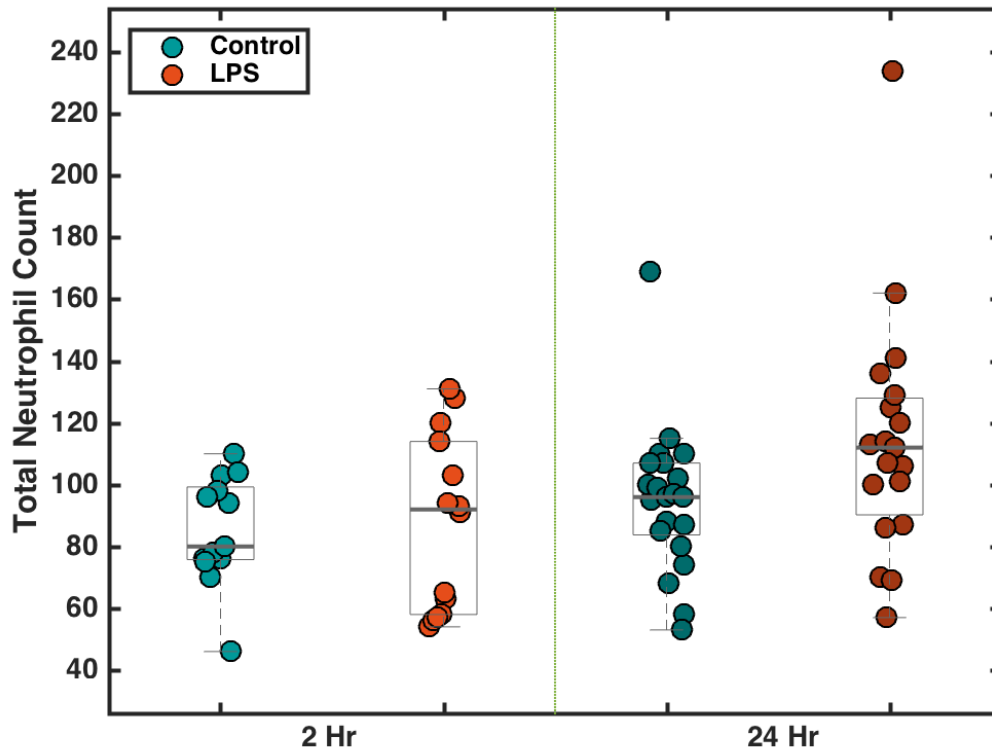


**Figure 4.4. Neutrophil counts after exposure to LPS.** The total number of neutrophils counted in larval zebrafish after exposure to LPS for 0 (control), 2, or 24 hours. At 2 hours post-exposure, there was no discernible difference between the LPS group and the control group. At 24 hours post-exposure, the LPS group displayed an increase in mean neutrophil count of  $1.2 \pm 0.1$ .

### 4.3 Materials and Methods

#### Hardware

The majority of the instrument was constructed with off the shelf parts. Custom parts were either laser cut from acrylic sheets or were 3D printed.

Fluorescence excitation is provided by various solid state lasers, selected by an acousto-optic tunable filter (AOTF, AA Opto-electronic) for coupling into a fiber launch to a galvanometer mirror (Cambridge Technology), which oscillates with a triangular waveform at 1 kHz to sweep the beam into a sheet. An objective lens (Mitutoyo 5X) and a prism route the sheet to the water-filled sample chamber where it intersects the specimen (Fig. 1). Detection is provided by a 20x water immersion objective (Olympus 20XW), mounted in the side of the chamber and sealed with an o-ring, its corresponding tube lens, and an sCMOS camera (Hamamatsu Orca Flash 4.0). Exposure times were 25 ms for all experiments presented here. Instrument control software was written in MATLAB.

#### Ethics statement

All zebrafish experiments were carried out in accordance with protocols approved by the University of Oregon Institutional Animal Care and Use Committee (Howe et al., 2013).

#### Zebrafish husbandry

The zebrafish line *Tg[BACmpo:gfp]* (Renshaw et al., 2006) was used for neutrophil imaging. Larval zebrafish were raised at a density of one embryo per milliliter and kept

at a constant temperature of 28 °C. Embryos were not fed during experiments and were sustained by their yolks.

### **Sample preparation**

Larval zebrafish were placed in dishes containing sterile embryo media with 0.05% methylcellulose and anaesthetized using 240 µg/ml tricaine methanesulfonate. This anaesthetic concentration is higher than the standard dosage, but was necessary likely because of permeation through the plastic tubing. Specimens are initially loaded into the tubing system by manual aspiration using a syringe connected to the opposite end of the tubing, maintaining a spacing between specimens of approximately 6 inches. Fish are pulled into the tubing head-first to ensure high and consistent flow speeds. (Fish travel better forwards than backwards). During experiments, larvae flowed through the tubing and were automatically stopped and positioned by a syringe pump and a series of valves. After imaging, larvae flowed into a dish containing sterile embryo medium.

### **LPS Treatment**

A filter-sterilized LPS (*E. coli* serotype 0111:B4, Sigma) solution was injected into flasks containing 15 MPO:GFP zebrafish larvae at 5 dpf for a final concentration of 150 µg/ml of LPS in each flask. Fish were incubated in the LPS solution for 2-24 hours as indicated in the text, after which they were removed from the solution and imaged.

## **Imaging Procedure**

For live imaging, each larval zebrafish flows through 0.7 mm inner diameter silicone tubing to a 50 mm long section of round 0.7 mm inner diameter, square exterior cross section, glass tubing in the specimen chamber. The contrast between the specimen and background in brightfield images is used to detect the specimen, stop the pump, and close off tubing using pinch valves to prevent specimen drift. Detecting the specimen and halting the flow places the specimen roughly within five millimeters of the desired location. Fine positioning of the specimen is performed by translating the specimen along the capillary axis (“x”) in roughly 30 steps of 0.3 mm size, capturing a brightfield image at each position, tiling the brightfield images into one large image, and comparing the result with a previously assembled “library” image. The comparison can be done in one of two ways, which yield indistinguishable positioning accuracies, both of which begin by averaging the image intensity along the “y” direction, giving a one-dimensional intensity profile. The profile is then compared with the profile derived from average library images either (i) by cross-correlation, in which one profile is offset in position and then multiplied by the other profile, and integrated (summed), giving a correlation value as a function of offset value, or (ii) the location of the profile’s intensity minimum is determined, and compared to the location of the average library profile’s minimum. In (i) the peak in the correlation function and in (ii) the difference between the minima gives the displacement between the profile and the library profile, and therefore indicates where the specimen should be precisely positioned. Following positioning, bright field illumination is switched off and the desired laser wavelength is selected by the AOTF. The *xyz* arm is then scanned perpendicular to the sheet plane, generating a 3D image

stack. The scan can be repeated for another region or another wavelength before the pump is directed to send the specimen out of the chamber, and bring in the next specimen.

### **Point Spread Function**

For measurements of the point spread function, 28 nm diameter fluorescent carboxylate-modified polystyrene spheres (Thermo Fisher cat. #F8787), with peak excitation and emission wavelengths 505 and 515 nm, respectively, were dispersed in oil with a similar index of refraction as water (Zeiss Immersol W 2010) inside the imaging capillaries. Three-dimensional scans were taken, with a z-spacing of 0.5  $\mu\text{m}$ .

### **Image-based neutrophil quantification**

Neutrophils were detected from image stacks using custom code written in Python, involving a coarse and fine thresholding. First, the 3D stack was thresholded using a low intensity value followed by the morphological operations of closing and erosion with structure elements of 1 pixel (Gonzalez and Woods, 2008). Connected above-threshold pixels were identified as objects using scikit-image's label function. Then, each detected object was further thresholded using an Otsu filter and labeled again. This re-thresholding process was repeated twice, and objects below 3  $\mu\text{m}^3$  were discarded as unphysical. The total intensity within each identified object represents the total fluorescence intensity of that neutrophil. For a full 3D dataset, the processing takes 1-2 minutes.

#### 4.4 Discussion

In recent years, many instruments for high content and high throughput imaging of small organisms, such as embryonic and larval zebrafish, have been developed (Gualda et al., 2015; Hwang and Lu, 2013; Letamendia et al., 2012; Liu et al., 2016; Pardo-Martin et al., 2010; Spomer et al., 2012; Westhoff et al., 2013; Yanik et al., 2011), and have demonstrated their utility for fast, accurate, imaging and screening. Our setup has similarities and differences to several of these, and advantages and disadvantages for particular applications. Several instruments are designed to image specimens held in multi-well plates (Letamendia et al., 2012; Liu et al., 2016; Spomer et al., 2012; Westhoff et al., 2013), including commercial instruments such as the ImageXpress High-Content Screening System ([CSL STYLE ERROR: reference with no printed form.]) and the Acquirer Imaging Machine (ACQUIFER). These plate-based systems enable integration with standard specimen containment, and also facilitate automated delivery of chemicals or other perturbations. Imaging is typically provided by widefield microscopy, which is rapid and simple but which prohibits three-dimensional imaging. While confocal microscopy is in principle possible, the thickness of standard plate bottoms would make this difficult except for specialized setups. Three-dimensional confocal fluorescence microscopy is, however, attained in automated instruments such as those of Refs. (Pardo-Martin et al., 2010) and the commercial VAST device (Biometrica, 2010), which use capillary- and tubing-based automated specimen handling and positioning. While successful, and enabling a wide range of studies, there are applications for which the advantages of light sheet microscopy compared to confocal microscopy, namely its rapid speed and low phototoxicity (Huisken, 2012; Jemielita et al., 2013; Keller et al., 2008,

2014; Power and Huisken, 2017; Santi, 2011), are important, such as the imaging of active cells in dynamic environments like the intestine. The requirement of orthogonal accessible light paths for light sheet imaging make its integration with existing high-throughput instruments non-trivial, motivating the work presented here. Our design of a relatively freestanding capillary amid a vertical excitation sheet and horizontal detection axis is effective, but it need not be the only solution. For example, one could imagine integration with single-lens-based light sheet techniques (Bouchard et al., 2015; Dunsby, 2008), and it will be interesting to see if such schemes are developed. We note that our device will have lower throughput than plate-based instruments, and will not integrate with commercial confocal microscopes as existing tubing-based methods do, but rather will enhance studies for which light sheet fluorescence microscopy allows insights into dynamic biological phenomena that are otherwise unattainable.

While our microscope is optimized for rapid imaging of larval zebrafish, the design is general and opens numerous possibilities for imaging a wide range of specimens, such as organoids, drosophila embryos, small marine invertebrates, and more, with the appropriate expansion of the positioning image library.

Our design does not rotate the specimen about the travel axis, a design choice that has advantages and disadvantages for applications. It is certainly possible to vary the specimen orientation by rotating the glass capillary, as, for example, in the VAST instrument (Biometrica, 2010). Rotation would enhance image quality, both by allowing the selection of particular orientations with minimal sheet distortion and by enabling the fusion of multiple views to gain isotropic resolution. We note, moreover, that variation in image quality due to the uncontrolled orientations of zebrafish likely contributes, along



with true biological variability, to the total scatter in neutrophil counts (Figs. 3, 4). The ability to examine a large number of specimens allows averaging over both sources of variation. Though it could be implemented, rotational positioning of each animal takes time and, at least in our design, significantly reduces the throughput of the instrument. Furthermore, we believe that many useful applications, e.g. the neutrophil counting demonstrated here, can be realized without specimen rotation, and that the simplicity of the setup as presented can hopefully foster widespread adoption. We note that rotation can be decoupled from the imaging area, as in Ref. (Biometrica, 2010), so that one specimen can be oriented while another is imaged, preventing a reduction in throughput. Such additions to the instrument described, though carrying a cost of greater complexity, may be worthwhile.

While the present design provides only a single three-dimensional image of each specimen, we envision future integration of a closed-loop fluidic circuit, with which specimens can be automatically loaded, imaged, and circulated repeatedly, allowing for high-throughput acquisition of multiple snapshots of the same specimen over time. In general, tackling the challenge of automated, high-throughput specimen handling will allow the technique of light sheet fluorescence microscopy to maximize its impact on the life sciences, and would be particularly useful for future experiments planned in the Parthasarathy Lab. These experiments, as well as a more in-depth discussion of improvements to the automated high-throughput light sheet microscope, are included in the following chapter.

## CHAPTER V

### DISCUSSION AND FUTURE WORK

#### **5.1 Introduction**

The preceding chapters have described completed experiments and a new instrument design, both of which hint at promising directions for the future. In this chapter, I will explore ongoing and future work related to those chapters. In particular, this chapter will focus on the immune system as an important area of study and an excellent starting point for building on previous work.

The immune system is important for understanding health, both because it is our major line of defense against pathogens and because it plays a role in complex health conditions such as autoimmune disorders, cancer therapies, and more. Zebrafish are an excellent model of the immune system because the basic components of the immune system are shared among vertebrates; zebrafish are a tractable, semi-transparent model organism that allows us to easily study all of these components. We will focus largely on the innate immune system, which is a nonspecific defense mechanism used to target bacteria. The innate immune system consists of several cell types, including neutrophils and macrophages, and signaling pathways including tumor necrosis factor alpha (tnfa). Transgenic zebrafish lines have been developed to visualize the aforementioned parts of the innate immune system: neutrophils (Renshaw et al., 2006), macrophages (Ellett et al., 2011), and tnfa (Nguyen-Chi et al.). Neutrophils are a highly motile type of white blood cell (Mayadas et al., 2014), and macrophages, similarly, are a type of white blood cell recruited to injury sites after neutrophils have responded (Prame Kumar et al., 2018).

Tnfa is a central inflammatory cytokine and indicator of many inflammatory responses (Parameswaran and Patial, 2010). By visualizing these inflammatory indicators, we can learn a great deal about host responses to bacteria, bacterial mechanisms, and other compounds.

Section 5.2 will focus on current and future work related to the *Vibrio cholerae* type VI secretion system, including the immune system as a possible pathway for the T6SS to increase gut motility in hosts. Section 5.3 will discuss improvements to the automated high-throughput light sheet microscope, including implementing a closed-loop system and developing a protocol for fast inflammation screening. Section 5.4 covers promising high-throughput experiments related to the immune system, including exploration of biological variations between fish and comparisons between imaging data and dissection data. Section 5.5 contains a summary, discussion, and concluding remarks.

## **5.2 Immune deficient zebrafish and the type VI secretion system**

In Chapter II, we learned that the *Vibrio cholerae* type VI secretion system (T6SS) can modulate host intestinal mechanics to displace other bacteria already present in the gut. However, an outstanding question remains: what pathway on the *host* side leads from bacterial T6SS activity in the intestine to increased gut motility in the host? The answer to this question is not obvious; somehow, information goes from bacteria inside the gut to peristaltic muscle contractions, and those muscle cells are not in contact with the interior of the gut! Likely candidates for this pathway include enteric neurons, goblet cells, and immune cells. Immune cells are a particularly likely candidate because they are known to respond to intestinal bacteria by increasing in number and migrating to

the gut. To begin exploring this question, we can use the wide variety of transgenic zebrafish lines available at the University of Oregon Zebrafish Facility. Zebrafish lines relevant to this question lack specific features that could play a role in the gut motility pathway; for example, fish with the *ret*<sup>hu2846</sup> mutant allele lack a functional enteric nervous system (ENS) (Heanue and Pachnis, 2008), and fish with a truncated version of myeloid differentiation factor 88 (MyD88) have a compromised immune system (van der Vaart et al., 2013). By repeating our T6SS experiments in these transgenic lines, we can determine whether these features play a role in translating T6SS activity to intestinal motility.

We chose MyD88 mutant zebrafish as a starting point for investigating the T6SS-gut motility pathway because prior studies have shown that general pro-inflammatory responses to bacteria are mediated by the MyD88 pathway (Bates et al., 2007; Cheesman et al., 2011). Also, the transgenic fish are already available! As an initial exploration, we mono-colonized germ-free MyD88 mutant larval zebrafish with either T6SS<sup>+</sup> or T6SS<sup>-</sup> *Vibrio cholerae* strains. These strains were identical to the strains discussed in Chapter III, and the experiment mirrored the procedures discussed in section 3.6. Figure 5.1 shows that T6SS<sup>+</sup>-inoculated fish show no increase in the amplitude of gut motility when compared to T6SS<sup>-</sup>-inoculated fish. This figure can be compared to Figure 3.4 (C), which shows that wild-type larval zebrafish show a large increase in gut motility when inoculated with T6SS<sup>+</sup> *V. cholerae*. Our initial data suggest that the immune system plays an important role in T6-mediated increases in gut motility, although more experiments will be needed to confirm this result, and to link MyD88 responses to particular cell types.

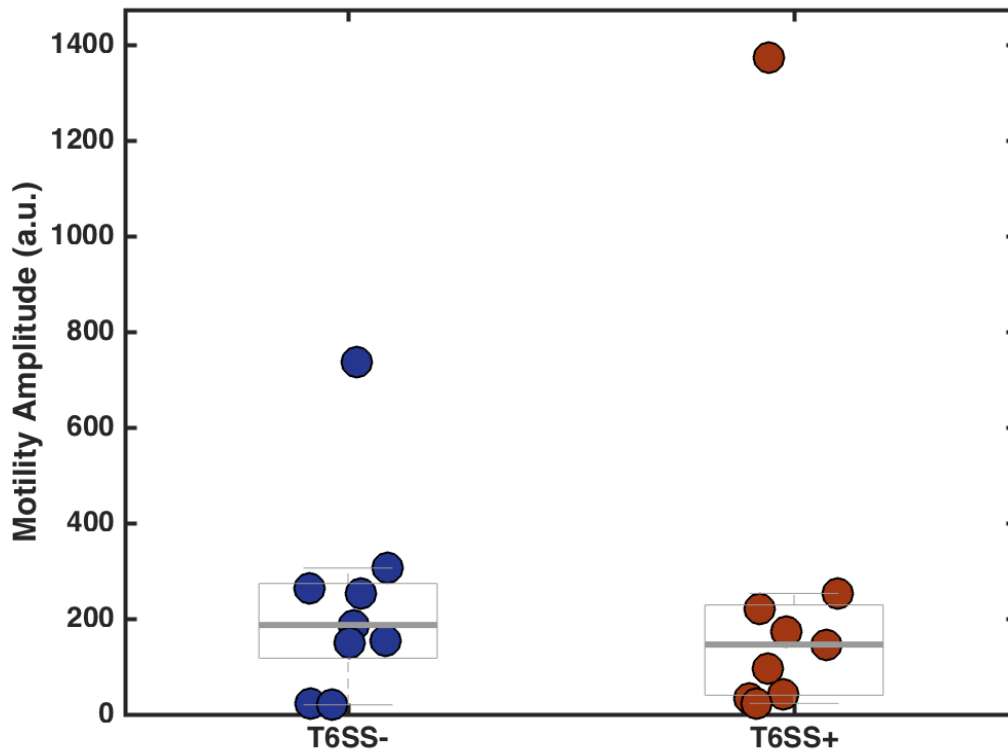


**Figure 5.1.** Gut motility amplitudes of MyD88 mutant zebrafish mono-associated with T6SS<sup>-</sup> and T6SS<sup>+</sup> *Vibrio cholerae* strains. Fish associated with the T6SS<sup>+</sup> strain show no changes in gut motility amplitude when compared to those associated with the T6SS<sup>-</sup> strain, demonstrating a major difference between wild-type and MyD88 mutant hosts (see also Section 3.5 and Figure 3.4).

Our initial results in MyD88 mutant zebrafish are a promising start, but there is much more work to be done on this topic in the future. First, experiments should be done to confirm the results described above. Second, single-cell RNA sequencing could provide fascinating insights into the changes in gene expression in host cells, which

would provide greater insights into the role of immune cells (or other cells) in the T6SS/gut motility pathway. Single-cell RNA sequencing provides the expression profile of individual cells using next generation sequencing technologies. Recently, researchers have used single cell RNA-seq on zebrafish to gain insights into the evolution of immune cell types (Carmona et al., 2017), and techniques have been developed to profile thousands of single cells in parallel (Zheng et al., 2017). Conveniently, the tools needed to carry out single cell RNA-seq experiments already exist in the University of Oregon Genomics Core. Finally, more broadly related to our T6SS work, invasion of multi-species communities should be explored. The gut microbiota is a complex community, so invasion of a more complex model community will give us better insights into the real-world dynamics of invasion by *Vibrio cholerae*. Furthermore, bacterial species respond differently to peristaltic motion depending on the physical structure of their communities in the gut; by observing invasion of a wider range of species, we will gain insights into which physical community structures are best (or worst) for expulsion due to gut motility. This experiment could be made easier with possible improvements to the automated high-throughput light sheet microscope, described below.

### **5.3 A high-throughput closed-loop design and inflammation screening protocols**

While the automated high-throughput light sheet microscope discussed in Chapter III is a significant step forward in microscope design, improvements to its hardware, software, and general protocols could vastly improve its functionality. In particular, implementing a closed-loop fluidic circuit would allow specimens to be automatically imaged repeatedly over many hours, which would expand the microscope's range of uses

to include extended live imaging experiments similar to those described in Chapter III. One possible design for this fluidic circuit, designed by Raghuv eer Parthasarathy, is shown in Figure 5.2.

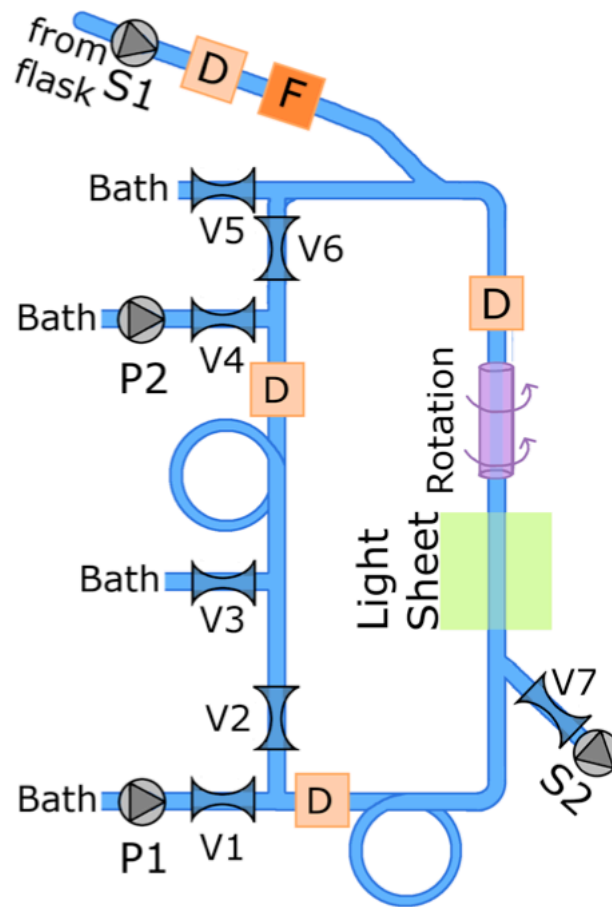


**Figure 5.2.** A possible schematic for closed-loop high-throughput imaging, designed by Raghuv eer Parthasarathy. Fish are pumped from a flask by a syringe pump (S1) through a discriminator (D) and fluorescence sorter (F), after which they enter the fluidic circuit. Valves (V) and

peristaltic pumps (P) direct the flow, and additional discriminators (D) sort fish for either repeated light sheet imaging or storage in fluid baths.

In addition to a closed-loop fluidic circuit, the high-throughput light sheet fluorescence microscope could greatly benefit from an established protocol and pipeline for imaging and analyzing inflammation or other immune responses in fish. The basic imaging pipeline is already in place for this development, but a great deal of refinement will be necessary before it is fully functional. Fish could be imaged as described in Chapter IV, and the data could be analyzed with (yet-to-be-written) software similar to the software for counting bacterial populations used in Chapter III, providing a fast and efficient method of screening for inflammation. The major improvements necessary for this pipeline will include establishing an imaging protocol and writing user-friendly software for analyzing the data. In terms of hardware, everything necessary is already in place, although improvements such as the addition of an automatic rotation arm and a longer tubing line for imaging more fish per run would add to its functionality. In spite of these potential improvements, the microscope is currently ready for basic experiments related to the immune system.

#### **5.4 High-throughput visualization of immune cells**

During and after improvements to the high-throughput light sheet microscope, initial experiments related to visualizing and studying the immune system can be performed. Foremost among these experiments is the comparison between total neutrophil counts in larval zebrafish when the gut is dissected and neutrophils are



manually counted versus when the fish are imaged and neutrophils are counted using software. The correspondence between neutrophils associated with dissected and intact intestines is not obvious. In dissection experiments, neutrophils must be attached to the gut with sufficient strength to be counted, and it is possible that these are a subset of those present in intact guts. Many experiments have used dissection and manual counting as the primary method of measuring neutrophil abundance (Rolig et al., 2015), so comparing light sheet data to dissection data will be both necessary for connecting our work to previous results and informative in its own right.

A second relatively easy high-throughput immune system experiment will involve imaging fish with fluorescently labeled neutrophils multiple times over the course of several days. By imaging the same fish more than once, we will determine how much of the variance in neutrophil counts is due to variation in individuals. This experiment is particularly exciting because it would not be possible using older methods of neutrophil quantification, i.e. dissection and manual counting. Related to this, phenotypical characterization of neutrophils within fish, such as morphological features and motility, would be possible using the same 3D data and would be both informative and important for understanding the specific effects of drugs and bacteria on neutrophils.

## **5.5 Summary and discussion**

The work presented here has spanned a wide range of topics, from experiments on bacterial mechanisms and their effects on live hosts, to instrument design, to possible experiments involving invasion of new communities, explorations of host genetic pathways, and visualizations of inflammation. The first two chapters discussed the

current state of host-microbiome and LSFM research and defined problems in those fields. Chapters III and IV addressed those issues through a series of experiments and the development of a new microscope. Chapter V has discussed potential directions for the future related to the previous topics, and should serve only as a starting point for a variety of exciting future experiments. In spite of the wide range of work in this dissertation, common themes can be found throughout. In particular, the use and development of advanced imaging techniques to make new biological discoveries has been an essential component of my work in graduate school. I am sure that research related to this theme will continue at the University of Oregon in the future, and I look forward to seeing the results.

## REFERENCES CITED

- Abu-Ali, G.S., Mehta, R.S., Lloyd-Price, J., Mallick, H., Branck, T., Ivey, K.L., Drew, D.A., DuLong, C., Rimm, E., Izard, J., et al. (2018). Metatranscriptome of human faecal microbial communities in a cohort of adult men. *Nat. Microbiol.* *3*, 356–366.
- ACQUIFER Screening. ACQUIFER. Available from: <https://www.acquifer.de/screening/>
- Adair, K.L., Wilson, M., Bost, A., and Douglas, A.E. (2018). Microbial community assembly in wild populations of the fruit fly *Drosophila melanogaster*. *ISME J.* *12*, 959–972.
- Almagro-Moreno, S., Pruss, K., and Taylor, R.K. (2015). Intestinal Colonization Dynamics of *Vibrio cholerae*. *PLoS Pathog.* *11*, e1004787.
- Anderson, M.C., Vonaesch, P., Saffarian, A., Marteyn, B.S., and Sansonetti, P.J. (2017). *Shigella sonnei* Encodes a Functional T6SS Used for Interbacterial Competition and Niche Occupancy. *Cell Host Microbe* *21*, 769-776.e3.
- Baker, R.P., Taormina, M.J., Jemielita, M., and Parthasarathy, R. (2015). A Combined Light Sheet Fluorescence and Differential Interference Contrast Microscope for Live Imaging of Multicellular Specimens. *J. Microsc.* *258*, 105–112.
- Bartlett, D.H., and Azam, F. (2005). Chitin, Cholera, and Competence. *Science* *310*, 1775–1777.
- Bartlett, T.M., Bratton, B.P., Duvshani, A., Miguel, A., Sheng, Y., Martin, N.R., Nguyen, J.P., Persat, A., Desmarais, S.M., VanNieuwenhze, M.S., et al. (2017). A Periplasmic Polymer Curves *Vibrio cholerae* and Promotes Pathogenesis. *Cell* *168*, 172-185.e15.
- Barzilay, E.J., Schaad, N., Magloire, R., Mung, K.S., Boney, J., Dahourou, G.A., Mintz, E.D., Steenland, M.W., Vertefeuille, J.F., and Tappero, J.W. (2013). Cholera Surveillance during the Haiti Epidemic — The First 2 Years. *N. Engl. J. Med.* *368*, 599–609.
- Bashiardes, S., Zilberman-Schapira, G., and Elinav, E. (2016). Use of Metatranscriptomics in Microbiome Research. *Bioinforma. Biol. Insights* *10*, 19–25.
- Bates, J.M., Mittge, E., Kuhlman, J., Baden, K.N., Cheesman, S.E., and Guillemin, K. (2006). Distinct signals from the microbiota promote different aspects of zebrafish gut differentiation. *Dev Biol* *297*, 374–386.
- Bates, J.M., Akerlund, J., Mittge, E., and Guillemin, K. (2007). Intestinal alkaline phosphatase detoxifies lipopolysaccharide and prevents inflammation in zebrafish in response to the gut microbiota. *Cell Host Microbe* *2*, 371–382.
- Benson, K.R. (2001). T. H. Morgan's resistance to the chromosome theory. *Nat. Rev. Genet.* *2*, 469–474.

Bernardy, E.E., Turnsek, M.A., Wilson, S.K., Tarr, C.L., and Hammer, B.K. (2016). Diversity of Clinical and Environmental Isolates of *Vibrio cholerae* in Natural Transformation and Contact-Dependent Bacterial Killing Indicative of Type VI Secretion System Activity. *Appl. Environ. Microbiol.* *82*, 2833–2842.

Biometrica, S. 180, Blackfly Interactive, Union (2010). Union Biometrica | VAST BioImager™ Platform Overview.

Borgeaud, S., Metzger, L.C., Scignari, T., and Blokesch, M. (2015). The type VI secretion system of *Vibrio cholerae* fosters horizontal gene transfer. *Science* *347*, 63–67.

Botstein, D., Chervitz, S.A., and Cherry, J.M. (1997). Yeast as a Model Organism. *Science* *277*, 1259–1260.

Bouchard, M.B., Voleti, V., Mendes, C.S., Lacefield, C., Grueber, W.B., Mann, R.S., Bruno, R.M., and Hillman, E.M.C. (2015). Swept confocally-aligned planar excitation (SCAPE) microscopy for high-speed volumetric imaging of behaving organisms. *Nat. Photonics* *9*, 113–119.

Buffie, C.G., Bucci, V., Stein, R.R., McKenney, P.T., Ling, L., Gobourne, A., No, D., Liu, H., Kinnebrew, M., Viale, A., et al. (2015). Precision microbiome reconstitution restores bile acid mediated resistance to *Clostridium difficile*. *Nature* *517*, 205–208.

Carmona, S.J., Teichmann, S.A., Ferreira, L., Macaulay, I.C., Stubbington, M.J.T., Cvejic, A., and Gfeller, D. (2017). Single-cell transcriptome analysis of fish immune cells provides insight into the evolution of vertebrate immune cell types. *Genome Res.* *27*, 451–461.

Chang, B.-J., Meza, V.D.P., and Stelzer, E.H.K. (2017). csiLSFM combines light-sheet fluorescence microscopy and coherent structured illumination for a lateral resolution below 100 nm. *Proc. Natl. Acad. Sci.* *114*, 4869–4874.

Chatzidaki-Livanis, M., Geva-Zatorsky, N., and Comstock, L.E. (2016). *Bacteroides fragilis* type VI secretion systems use novel effector and immunity proteins to antagonize human gut Bacteroidales species. *Proc. Natl. Acad. Sci.* *113*, 3627–3632.

Cheesman, S.E., Neal, J.T., Mittge, E., Seredick, B.M., and Guillemin, K. (2011). Epithelial cell proliferation in the developing zebrafish intestine is regulated by the Wnt pathway and microbial signaling via Myd88. *Proc Natl Acad Sci USA* *108*, 4570–4577.

Chen, B.-C., Legant, W.R., Wang, K., Shao, L., Milkie, D.E., Davidson, M.W., Janetopoulos, C., Wu, X.S., Hammer, J.A., Liu, Z., et al. (2014). Lattice light-sheet microscopy: Imaging molecules to embryos at high spatiotemporal resolution. *Science* *346*, 1257998.

Choi, K.-H., Gaynor, J.B., White, K.G., Lopez, C., Bosio, C.M., Karkhoff-Schweizer, R.R., and Schweizer, H.P. (2005). A Tn7-based broad-range bacterial cloning and expression system. *Nat. Methods* *2*, 443–448.

Cohen, B.J., and Loew, F.M. (1984). Chapter 1 - Laboratory Animal Medicine: Historical Perspectives. In *Laboratory Animal Medicine*, J.G. Fox, B.J. Cohen, and F.M. Loew, eds. (Academic Press), pp. 1–17.

Consortium, T.H.M.P. (2012). Structure, function and diversity of the healthy human microbiome. *Nature* *486*, 207–214.

Coyne, M.J., Zitomersky, N.L., McGuire, A.M., Earl, A.M., and Comstock, L.E. (2014). Evidence of Extensive DNA Transfer between Bacteroidales Species within the Human Gut. *MBio* *5*, e01305-14.

Cremer, J., Segota, I., Yang, C., Arnoldini, M., Sauls, J.T., Zhang, Z., Gutierrez, E., Groisman, A., and Hwa, T. (2016). Effect of flow and peristaltic mixing on bacterial growth in a gut-like channel. *Proc. Natl. Acad. Sci.* *113*, 11414–11419.

Cremer, J., Arnoldini, M., and Hwa, T. (2017). Effect of water flow and chemical environment on microbiota growth and composition in the human colon. *Proc. Natl. Acad. Sci.* *114*, 6438–6443.

David, L.A., Weil, A., Ryan, E.T., Calderwood, S.B., Harris, J.B., Chowdhury, F., Begum, Y., Qadri, F., LaRocque, R.C., and Turnbaugh, P.J. (2015). Gut Microbial Succession Follows Acute Secretory Diarrhea in Humans. *MBio* *6*, e00381-15.

Dobson, A.J., Chaston, J.M., and Douglas, A.E. (2016). The *Drosophila* transcriptional network is structured by microbiota. *BMC Genomics* *17*, 975.

Dooley, K., and Zon, L.I. (2000). Zebrafish: a model system for the study of human disease. *Curr. Opin. Genet. Dev.* *10*, 252–256.

Dunsby, C. (2008). Optically sectioned imaging by oblique plane microscopy. *Opt. Express* *16*, 20306–20316.

Ellett, F., Pase, L., Hayman, J.W., Andrianopoulos, A., and Lieschke, G.J. (2011). mpeg1 promoter transgenes direct macrophage-lineage expression in zebrafish. *Blood* *117*, e49–e56.

Fei, P., Lee, J., Packard, R.R.S., Sereti, K.-I., Xu, H., Ma, J., Ding, Y., Kang, H., Chen, H., Sung, K., et al. (2016). Cardiac Light-Sheet Fluorescent Microscopy for Multi-Scale and Rapid Imaging of Architecture and Function. *Sci. Rep.* *6*, 22489.

Foster, K.R., Schluter, J., Coyte, K.Z., and Rakoff-Nahoum, S. (2017). The evolution of the host microbiome as an ecosystem on a leash. *Nature* *548*, 43–51.

Fu, Y., Waldor, M.K., and Mekalanos, J.J. (2013). Tn-Seq Analysis of *Vibrio cholerae* Intestinal Colonization Reveals a Role for T6SS-Mediated Antibacterial Activity in the Host. *Cell Host Microbe* *14*, 652–663.

Galindo-Villegas, J. (2016). Recent findings on vertebrate developmental immunity using the zebrafish model. *Mol. Immunol.* *69*, 106–112.

Ganz, J., Baker, R.P., Hamilton, M.K., Melancon, E., Diba, P., Eisen, J.S., and Parthasarathy, R. (2018). Image velocimetry and spectral analysis enable quantitative characterization of larval zebrafish gut motility. *Neurogastroenterol. Motil.* *30*, e13351.

Gonzalez, R.C., and Woods, R.E. (2008). *Digital Image Processing* (Upper Saddle River, N.J.: Prentice Hall).

Gualda, E.J., Pereira, H., Vale, T., Estrada, M.F., Brito, C., and Moreno, N. (2015). SPIM-fluid: open source light-sheet based platform for high-throughput imaging. *Biomed. Opt. Express* *6*, 4447–4456.

Haas, L. (2001). Emil Adolph von Behring (1854–1917) and Shibasaburo Kitasato (1852–1931). *J. Neurol. Neurosurg. Psychiatry* *71*, 62–62.

Hachani, A., Wood, T.E., and Filloux, A. (2016). Type VI secretion and anti-host effectors. *Curr. Opin. Microbiol.* *29*, 81–93.

Halpern, M., and Izhaki, I. (2017). Fish as Hosts of *Vibrio cholerae*. *Front. Microbiol.* *8*.

Harris, J.B., LaRocque, R.C., Qadri, F., Ryan, E.T., and Calderwood, S.B. (2012). Cholera. *Lancet* *379*, 2466–2476.

Heanue, T.A., and Pachnis, V. (2008). Ret isoform function and marker gene expression in the enteric nervous system is conserved across diverse vertebrate species. *Mech. Dev.* *125*, 687–699.

Hill, J.H., Franzosa, E.A., Huttenhower, C., and Guillemin, K. (2016). A conserved bacterial protein induces pancreatic beta cell expansion during zebrafish development.

Ho, B.T., Dong, T.G., and Mekalanos, J.J. (2014). A View to a Kill: The Bacterial Type VI Secretion System. *Cell Host Microbe* *15*, 9–21.

Howe, D.G., Bradford, Y.M., Conlin, T., Eagle, A.E., Fashena, D., Frazer, K., Knight, J., Mani, P., Martin, R., Moxon, S.A.T., et al. (2013). ZFIN, the Zebrafish Model Organism Database: increased support for mutants and transgenics. *Nucleic Acids Res.* *41*, D854–860.

Hsiao, A., Ahmed, A.M.S., Subramanian, S., Griffin, N.W., Drewry, L.L., Petri, W.A., Haque, R., Ahmed, T., and Gordon, J.I. (2014). Members of the human gut microbiota involved in recovery from *Vibrio cholerae* infection. *Nature* *515*, 423–426.

Huisken, J. (2012). Slicing embryos gently with laser light sheets. *BioEssays* *34*.

Hwang, H., and Lu, H. (2013). Microfluidic tools for developmental studies of small model organisms — nematodes, fruit flies, and zebrafish. *Biotechnol. J.* *8*, 192–205.

Jemielita, M., Taormina, M.J., Delaurier, A., Kimmel, C.B., and Parthasarathy, R. (2013). Comparing phototoxicity during the development of a zebrafish craniofacial bone using confocal and light sheet fluorescence microscopy techniques. *J. Biophotonics* 6, 920–928.

Jemielita, M., Taormina, M.J., Burns, A.R., Hampton, J.S., Rolig, A.S., Guillemin, K., and Parthasarathy, R. (2014). Spatial and Temporal Features of the Growth of a Bacterial Species Colonizing the Zebrafish Gut. *MBio* 5, e01751-14.

Jennings, B.H. (2011). *Drosophila* – a versatile model in biology & medicine. *Mater. Today* 14, 190–195.

Joshi, A., Kostiuk, B., Rogers, A., Teschler, J., Pukatzki, S., and Yildiz, F.H. (2017). Rules of Engagement: The Type VI Secretion System in *Vibrio cholerae*. *Trends Microbiol.* 25, 267–279.

Kadirkamanathan, V., Anderson, S.R., Billings, S.A., Zhang, X., Holmes, G.R., Reyes-Aldasoro, C.C., Elks, P.M., and Renshaw, S.A. (2012). The Neutrophil's Eye-View: Inference and Visualisation of the Chemoattractant Field Driving Cell Chemotaxis In Vivo. *PLoS ONE* 7, e35182.

Kanther, M., Tomkovich, S., Xiaolun, S., Grosser, M.R., Koo, J., Flynn, E.J., Jobin, C., and Rawls, J.F. (2014). Commensal microbiota stimulate systemic neutrophil migration through induction of serum amyloid A. *Cell. Microbiol.* 16, 1053–1067.

Keller, P.J. (2013). Imaging Morphogenesis: Technological Advances and Biological Insights. *Science* 340, 1234168.

Keller, P.J., and Ahrens, M.B. (2015). Visualizing Whole-Brain Activity and Development at the Single-Cell Level Using Light-Sheet Microscopy. *Neuron* 85, 462–483.

Keller, P.J., Schmidt, A.D., Wittbrodt, J., and Stelzer, E.H.K. (2008). Reconstruction of Zebrafish Early Embryonic Development by Scanned Light Sheet Microscopy. *Science* 322, 1065–1069.

Keller, P.J., Ahrens, M.B., and Freeman, J. (2014). Light-sheet imaging for systems neuroscience.

Khairy, K., Lemon, W.C., Amat, F., and Keller, P.J. (2015). Light sheet-based imaging and analysis of early embryogenesis in the fruit fly. *Methods Mol. Biol. Clifton NJ* 1189, 79–97.

Laviad -Shitrit, S., Lev-Ari, T., Katzir, G., Sharaby, Y., Izhaki, I., and Halpern, M. (2017). Great cormorants (*Phalacrocorax carbo*) as potential vectors for the dispersal of *Vibrio cholerae*. *Sci. Rep.* 7, 7973.

Lescak, E.A., and Milligan-Myhre, K.C. (2017). Teleosts as Model Organisms To Understand Host-Microbe Interactions. *J. Bacteriol.* 199, e00868-16.

Letamendia, A., Quevedo, C., Ibarbia, I., Virto, J.M., Holgado, O., Diez, M., Belmonte, J.C.I., and Callol-Massot, C. (2012). Development and Validation of an Automated High-Throughput System for Zebrafish In Vivo Screenings. *PLOS ONE* 7, e36690.

Liu, T.-L., Upadhyayula, S., Milkie, D.E., Singh, V., Wang, K., Swinburne, I.A., Mosaliganti, K.R., Collins, Z.M., Hiscock, T.W., Shea, J., et al. (2018). Observing the cell in its native state: Imaging subcellular dynamics in multicellular organisms. *Science* 360, eaaq1392.

Liu, X., Painter, R.E., Enesa, K., Holmes, D., Whyte, G., Garlisi, C.G., Monsma, F.J., Rehak, M., Craig, F.F., and Smith, C.A. (2016). High-throughput screening of antibiotic-resistant bacteria in picodroplets. *Lab. Chip* 16, 1636–1643.

Logan, S.L., Thomas, J., Yan, J., Baker, R.P., Shields, D.S., Xavier, J.B., Hammer, B.K., and Parthasarathy, R. (2018). The *Vibrio cholerae* type VI secretion system can modulate host intestinal mechanics to displace gut bacterial symbionts. *Proc. Natl. Acad. Sci.* 115, E3779–E3787.

Ma, A.T., and Mekalanos, J.J. (2010). In vivo actin cross-linking induced by *Vibrio cholerae* type VI secretion system is associated with intestinal inflammation. *Proc. Natl. Acad. Sci.* 107, 4365–4370.

Martinson, V.G., Douglas, A.E., and Jaenike, J. (2017). Community structure of the gut microbiota in sympatric species of wild *Drosophila*. *Ecol. Lett.* 20, 629–639.

Mayadas, T.N., Cullere, X., and Lowell, C.A. (2014). The multifaceted functions of neutrophils. *Annu. Rev. Pathol.* 9, 181–218.

McDole, K., Guignard, L., Amat, F., Berger, A., Malandain, G., Royer, L.A., Turaga, S.C., Branson, K., and Keller, P.J. (2018). In Toto Imaging and Reconstruction of Post-Implantation Mouse Development at the Single-Cell Level. *Cell* 175, 859-876.e33.

McNally, L., Bernardy, E., Thomas, J., Kalziqui, A., Pentz, J., Brown, S.P., Hammer, B.K., Yunker, P.J., and Ratcliff, W.C. (2017). Killing by Type VI secretion drives genetic phase separation and correlates with increased cooperation. *Nat. Commun.* 8, ncomms14371.

Meijer, A.H., and Spaink, H.P. (2011). Host-pathogen interactions made transparent with the zebrafish model. *Curr. Drug Targets* 12, 1000–1017.

Milligan-Myhre, K., Charette, J.R., Phennicie, R.T., Stephens, W.Z., Rawls, J.F., Guillemain, K., and Kim, C.H. (2011). Chapter 4 - Study of Host–Microbe Interactions in Zebrafish. In *Methods in Cell Biology*, H.W. Detrich, M. Westerfield, and L.I. Zon, eds. (Academic Press), pp. 87–116.

Mitchell, K.C., Breen, P., Britton, S., Neely, M.N., and Withey, J.H. (2017). Quantifying *Vibrio cholerae* enterotoxicity in a zebrafish infection model. *Appl. Environ. Microbiol.* AEM.00783-17.



- Nguyen, T.L.A., Vieira-Silva, S., Liston, A., and Raes, J. (2015). How informative is the mouse for human gut microbiota research? *Dis. Model. Mech.* *8*, 1–16.
- Nguyen-Chi, M., Laplace-Builhe, B., Travnickova, J., Luz-Crawford, P., Tejedor, G., Phan, Q.T., Duroux-Richard, I., Levraud, J.-P., Kissa, K., Lutfalla, G., et al. Identification of polarized macrophage subsets in zebrafish. *ELife* *4*.
- Oehlers, S.H., Flores, M.V., Okuda, K.S., Hall, C.J., Crosier, K.E., and Crosier, P.S. (2011). A chemical enterocolitis model in zebrafish larvae that is dependent on microbiota and responsive to pharmacological agents. *Dev. Dyn.* *240*, 288–298.
- Orata, F.D., Keim, P.S., and Boucher, Y. (2014). The 2010 Cholera Outbreak in Haiti: How Science Solved a Controversy. *PLoS Pathog.* *10*.
- Parameswaran, N., and Patial, S. (2010). Tumor Necrosis Factor- $\alpha$  Signaling in Macrophages. *Crit. Rev. Eukaryot. Gene Expr.* *20*, 87–103.
- Pardo-Martin, C., Chang, T.-Y., Koo, B.K., Gilleland, C.L., Wasserman, S.C., and Yanik, M.F. (2010). High-throughput *in vivo* vertebrate screening. *Nat. Methods* *7*, 634–636.
- Parthasarathy, R. (2018). Monitoring microbial communities using light sheet fluorescence microscopy. *Curr. Opin. Microbiol.* *43*, 31–37.
- Perlman, R.L. (2016). Mouse models of human disease. *Evol. Med. Public Health* *2016*, 170–176.
- Power, R.M., and Huisken, J. (2017). A guide to light-sheet fluorescence microscopy for multiscale imaging. *Nat. Methods* *14*, 360–373.
- Pradeep Kumar, K., Nicholls, A.J., and Wong, C.H.Y. (2018). Partners in crime: neutrophils and monocytes/macrophages in inflammation and disease. *Cell Tissue Res.* *371*, 551–565.
- Pruzzo, C., Vezzulli, L., and Colwell, R.R. (2008). Global impact of *Vibrio cholerae* interactions with chitin. *Environ. Microbiol.* *10*, 1400–1410.
- Pukatzki, S., Ma, A.T., Sturtevant, D., Krastins, B., Sarracino, D., Nelson, W.C., Heidelberg, J.F., and Mekalanos, J.J. (2006). Identification of a conserved bacterial protein secretion system in *Vibrio cholerae* using the *Dictyostelium* host model system. *Proc. Natl. Acad. Sci.* *103*, 1528–1533.
- Rajilić-Stojanović, M., Heilig, H.G.H.J., Tims, S., Zoetendal, E.G., and de Vos, W.M. (2013). Long-term monitoring of the human intestinal microbiota composition. *Environ. Microbiol.* *15*, 1146–1159.
- Renshaw, S.A., Loynes, C.A., Trushell, D.M.I., Elworthy, S., Ingham, P.W., and Whyte, M.K.B. (2006). A transgenic zebrafish model of neutrophilic inflammation. *Blood* *108*, 3976–3978.

- Riddle, D.L., Blumenthal, T., Meyer, B.J., and Priess, J.R. (1997). *The Biological Model* (Cold Spring Harbor Laboratory Press).
- Rolig, A.S., Parthasarathy, R., Burns, A.R., Bohannan, B.J.M., and Guillemin, K. (2015). Individual Members of the Microbiota Disproportionately Modulate Host Innate Immune Responses. *Cell Host Microbe* *18*, 613–620.
- Runft, D.L., Mitchell, K.C., Abuaita, B.H., Allen, J.P., Bajer, S., Ginsburg, K., Neely, M.N., and Withey, J.H. (2014). Zebrafish as a Natural Host Model for *Vibrio cholerae* Colonization and Transmission. *Appl. Environ. Microbiol.* *80*, 1710–1717.
- Russell, A.B., Wexler, A.G., Harding, B.N., Whitney, J.C., Bohn, A.J., Goo, Y.A., Tran, B.Q., Barry, N.A., Zheng, H., Peterson, S.B., et al. (2014a). A Type VI Secretion-Related Pathway in Bacteroidetes Mediates Interbacterial Antagonism. *Cell Host Microbe* *16*, 227–236.
- Russell, A.B., Peterson, S.B., and Mougous, J.D. (2014b). Type VI secretion system effectors: poisons with a purpose. *Nat. Rev. Microbiol.* *12*, nrmicro3185.
- Sana, T.G., Flaugnatti, N., Lugo, K.A., Lam, L.H., Jacobson, A., Baylot, V., Durand, E., Journet, L., Cascales, E., and Monack, D.M. (2016). *Salmonella Typhimurium* utilizes a T6SS-mediated antibacterial weapon to establish in the host gut. *Proc. Natl. Acad. Sci.* *113*, E5044–E5051.
- Santi, P.A. (2011). Light Sheet Fluorescence Microscopy. *J. Histochem. Cytochem.* *59*, 129–138.
- Siedentopf, H., and Zsigmondy, R. (1902). Über Sichtbarmachung und Größenbestimmung ultramikroskopischer Teilchen, mit besonderer Anwendung auf Goldrubingläser. *Ann. Phys.* *315*, 1–39.
- Silva, A.J., and Benitez, J.A. (2016). *Vibrio cholerae* Biofilms and Cholera Pathogenesis. *PLoS Negl. Trop. Dis.* *10*, e0004330.
- Spees, A.M., Lopez, C.A., Kingsbury, D.D., Winter, S.E., and Bäumlner, A.J. (2013). Colonization Resistance: Battle of the Bugs or Ménage à Trois with the Host? *PLOS Pathog.* *9*, e1003730.
- Spomer, W., Pfriem, A., Alshut, R., Just, S., and Pylatiuk, C. (2012). High-throughput screening of zebrafish embryos using automated heart detection and imaging. *J. Lab. Autom.* *17*, 435–442.
- Stefaniuk, M., Gualda, E.J., Pawlowska, M., Legutko, D., Matryba, P., Koza, P., Konopka, W., Owczarek, D., Wawrzyniak, M., Loza-Alvarez, P., et al. (2016). Light-sheet microscopy imaging of a whole cleared rat brain with Thy1-GFP transgene. *Sci. Rep.* *6*, 28209.

- Streilein, J.W. (1965). Give and Take: The Development of Tissue Transplantation. Francis D. Moore. Saunders, Philadelphia, 1964. xii + 182 pp. Illus. \$5.50. *Science* 148, 1317–1317.
- Tang, W.J., Fernandez, J.G., Sohn, J.J., and Amemiya, C.T. (2015). Chitin Is Endogenously Produced in Vertebrates. *Curr. Biol.* 25, 897–900.
- Taormina, M.J., Jemielita, M., Stephens, W.Z., Burns, A.R., Troll, J.V., Parthasarathy, R., and Guillemin, K. (2012). Investigating Bacterial-Animal Symbioses with Light Sheet Microscopy. *Biol. Bull.* 223, 7–20.
- Thelin, K.H., and Taylor, R.K. (1996). Toxin-coregulated pilus, but not mannose-sensitive hemagglutinin, is required for colonization by *Vibrio cholerae* O1 El Tor biotype and O139 strains. *Infect. Immun.* 64, 2853–2856.
- Tomer, R., Khairy, K., Amat, F., and Keller, P.J. (2012). Quantitative high-speed imaging of entire developing embryos with simultaneous multiview light-sheet microscopy. *Nat. Methods* 9, 755–763.
- Truong, T.V., Supatto, W., Koos, D.S., Choi, J.M., and Fraser, S.E. (2011). Deep and fast live imaging with two-photon scanned light-sheet microscopy. *Nat. Methods* 8, 757–760.
- Udan, R.S., Piazza, V.G., Hsu, C., Hadjantonakis, A.-K., and Dickinson, M.E. (2014). Quantitative imaging of cell dynamics in mouse embryos using light-sheet microscopy. *Development* 141, 4406–4414.
- van der Vaart, M., van Soest, J.J., Spaik, H.P., and Meijer, A.H. (2013). Functional analysis of a zebrafish *myd88* mutant identifies key transcriptional components of the innate immune system. *Dis. Model. Mech.* 6, 841–854.
- Vega, N.M., and Gore, J. (2017). Stochastic assembly produces heterogeneous communities in the *Caenorhabditis elegans* intestine. *PLOS Biol.* 15, e2000633.
- Verster, A.J., Ross, B.D., Radey, M.C., Bao, Y., Goodman, A.L., Mougous, J.D., and Borenstein, E. (2017). The Landscape of Type VI Secretion across Human Gut Microbiomes Reveals Its Role in Community Composition. *Cell Host Microbe* 22, 411–419.e4.
- Voie, A.H., Burns, D.H., and Spelman, F.A. (1993). Orthogonal-plane fluorescence optical sectioning: Three-dimensional imaging of macroscopic biological specimens. *J. Microsc.* 170, 229–236.
- van der Waaij, D., Vries, J.M.B., and der Wees, J.E.C.L. (1971). Colonization resistance of the digestive tract in conventional and antibiotic-treated mice. *J. Hyg. (Lond.)* 69, 405–411.

- Watve, S.S., Thomas, J., and Hammer, B.K. (2015). CytR Is a Global Positive Regulator of Competence, Type VI Secretion, and Chitinases in *Vibrio cholerae*. *PLOS ONE* *10*, e0138834.
- Weber, M., Scherf, N., Meyer, A.M., Panáková, D., Kohl, P., and Huisken, J. (2017). Cell-accurate optical mapping across the entire developing heart. *ELife* *6*, e28307.
- Westhoff, J.H., Giselbrecht, S., Schmidts, M., Schindler, S., Beales, P.L., Tönshoff, B., Liebel, U., and Gehrig, J. (2013). Development of an Automated Imaging Pipeline for the Analysis of the Zebrafish Larval Kidney. *PLOS ONE* *8*, e82137.
- Wexler, A.G., Bao, Y., Whitney, J.C., Bobay, L.-M., Xavier, J.B., Schofield, W.B., Barry, N.A., Russell, A.B., Tran, B.Q., Goo, Y.A., et al. (2016). Human symbionts inject and neutralize antibacterial toxins to persist in the gut. *Proc. Natl. Acad. Sci.* *113*, 3639–3644.
- Wiles, T.J., Jemielita, M., Baker, R.P., Schlomann, B.H., Logan, S.L., Ganz, J., Melancon, E., Eisen, J.S., Guillemin, K., and Parthasarathy, R. (2016). Host Gut Motility Promotes Competitive Exclusion within a Model Intestinal Microbiota. *PLOS Biol.* *14*, e1002517.
- Wiles, T.J., Wall, E.S., Schlomann, B.H., Hay, E.A., Parthasarathy, R., and Guillemin, K. (2017). Modernized tools for streamlined genetic manipulation of wild and diverse symbiotic bacteria. *BioRxiv* 202861.
- Yanik, M.F., Rohde, C.B., and Pardo-Martin, C. (2011). Technologies for Micromanipulating, Imaging, and Phenotyping Small Invertebrates and Vertebrates. *Annu. Rev. Biomed. Eng.* *13*, 185–217.
- Yilmaz, L.S., and Walhout, A.J.M. (2014). Worms, bacteria, and micronutrients: an elegant model of our diet. *Trends Genet.* *30*, 496–503.
- Young, V.B. (2017). The role of the microbiome in human health and disease: an introduction for clinicians. *BMJ* *356*, j831.
- Zac Stephens, W., Burns, A.R., Stagaman, K., Wong, S., Rawls, J.F., Guillemin, K., and Bohannan, B.J.M. (2016). The composition of the zebrafish intestinal microbial community varies across development. *ISME J.* *10*, 644–654.
- Zhao, W., Caro, F., Robins, W., and Mekalanos, J.J. (2018). Antagonism toward the intestinal microbiota and its effect on *Vibrio cholerae* virulence. *Science* *359*, 210–213.
- Zheng, G.X.Y., Terry, J.M., Belgrader, P., Ryvkin, P., Bent, Z.W., Wilson, R., Ziraldo, S.B., Wheeler, T.D., McDermott, G.P., Zhu, J., et al. (2017). Massively parallel digital transcriptional profiling of single cells. *Nat. Commun.* *8*, 14049.

Zheng, J., Ho, B., and Mekalanos, J.J. (2011). Genetic Analysis of Anti-Amoebae and Anti-Bacterial Activities of the Type VI Secretion System in *Vibrio cholerae*. PLOS ONE 6, e23876.

Zuckerman, J.N., Rombo, L., and Fisch, A. (2007). The true burden and risk of cholera: implications for prevention and control. Lancet Infect. Dis. 7, 521–530.

ImageXpress Micro XLS Widefield High-Content Analysis System | Molecular Devices.